Molecular Diversity (2023) 27:2577–2603
https://doi.org/10.1007/s11030-022-10570-x

ORIGINAL ARTICLE

Nanobody-peptide-conjugate (NPC) for passive immunotherapy against SARS-CoV-2 variants of concern (VoC): a prospective pan-coronavirus therapeutics

Mamta Panda[1] · Elora Kalita[1] · Satyendra Singh[1] · Ketan Kumar[1] · Vijay Kumar Prajapati[1]

Received: 6 October 2022 / Accepted: 11 November 2022 / Published online: 18 November 2022

Abstract

The COVID-19 crisis, incited by the zoonotic SARS-CoV-2 virus, has quickly escalated into a catastrophic public health issue and a grave threat to humankind owing to the advent of mutant viruses. Multiple pharmaceutical therapies or biologics envision stopping the virus from spreading further; however, WHO has voiced concerns about the variants of concern (VoCs) inability to respond. Nanobodies are a new class of antibody mimics with binding affinity and specificity similar to classical mAbs, as well as the privileges of a small molecular weight, ease of entry into solid tissues, and binding cryptic epitopes of the antigen. Herein, we investigated multiple putative anti-SARS-CoV-2 nanobodies targeting the Receptor binding domain of the WHO-listed SARS-CoV-2 variants of concern using a comprehensive computational immunoinformatics methodology. With affinity maturation via alanine scanning mutagenesis, we remodeled an ultrapotent nanobody with substantial breadth and potency, exhibiting pico-molar binding affinities against all the VoCs. An antiviral peptide with specificity for ACE-2 receptors was affixed to make it multispecific and discourage viral entry. Collectively, we constructed a broad-spectrum therapeutic biparatopic nanobody-peptide conjugate (NPC) extending coverage to SARS-CoV-2 VoCs RBDs. We PEGylated the biparatopic construct with 20kD maleimide-terminated PEG (MAL-(PEG)n-OMe) to improve its clinical efficacy limiting rapid renal clearance, and performed in silico cloning to facilitate future experimental studies. Our findings suggest that combining biparatopic nanobody conjugate with standard treatment may be a promising bivariate tool for combating viral entry during COVID-19 illness.

✉ Vijay Kumar Prajapati
vijay84bhu@gmail.com

[1] Department of Biochemistry, School of Life Sciences, Central University of Rajasthan, Bandarsindri, Kishangarh, Ajmer, Rajasthan 305817, India

Graphical abstract

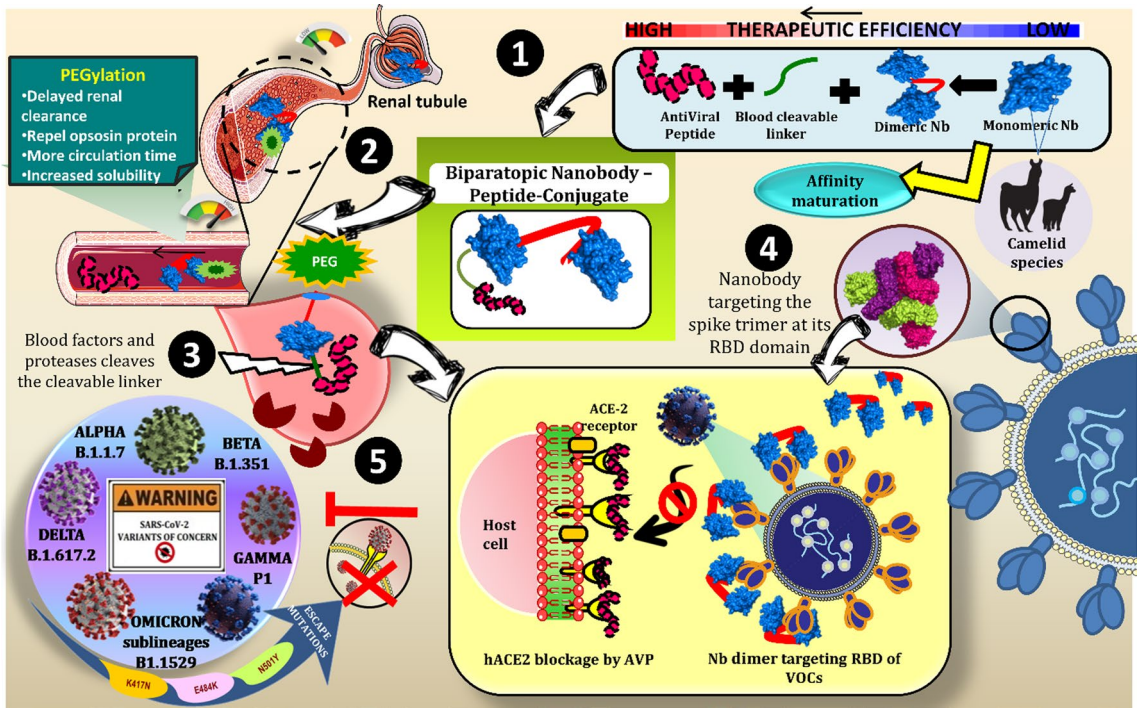

Keywords Nanobody · Nanobody conjugate · SARS-CoV-2 VoCs · Alanine scanning · Epitope mapping

Introduction

Since the introduction of COVID-19, the world has already gone in face of three deadly outbursts of the pandemic wave, becoming the prime cause of the global health crisis of the twenty-first century. The World Health Organization (WHO) initially familiarized the Severe Acute Respiratory Syndrome Coronavirus 2 (SARS-CoV-2) or COVID-19 in Wuhan City, Hubei Province, China, on December 30, 2019, quoting it as unusual viral pneumonia of unclear etiology. It is already successful in spreading across 226 countries, raising the death toll to more than 6.3 million deaths. Reports have acknowledged the emergence of seven coronaviruses that infect the human host, of which SARS-CoV-2 has proven to be fatal. Throughout this pandemic, the zoonotic SARS-CoV-2 has continuously evolved by undergoing genetic mutations during its replication cycle, thereby circulating nationwide. With the advent of the Global Initiative on Sharing All Influenza Data (GISAID), it has become easy to access the viral genomic database, which is growing exponentially [1]. This scheme keeps real-time surveillance of the international viral transmission, which helps to keep track of the epidemiological situation of emerging SARS CoV-2 variants and the associated mutation, which boosts the pathogen's virulence. The scientific community is consistently recording the amino acid changes acquired by the evolving SARS CoV-2 virus accounting for expanding epidemiological features since December 2019.

Given the dynamic nature of the SARS-CoV-2 variants, WHO convened a group of authorities to classify these variants based on increased impact and risk caused to public health into- variants of concern (VOC), Variants of Interest (VOI), and Variants under monitor (VUM) [2]. Primarily the Variant of Concerns is known to stagnate the COVID-19 outburst, evidenced by increased transmissibility, disease severity, fall in the neutralization ability by the antibodies, and decreased effectiveness of the administered vaccine and diagnostic failures. Currently reported VoCs include Alpha (B. 1. 1. 7), Beta (B. 1.351), Gamma (P.1), Delta (B.1.617.2), and Omicron (B.1.1.529) and its sub-lineages [BA.1, BA.2, BA.3 (recombinant XE)]. Mutants designated as Variants of Interest or Variants under Monitoring have a potent force in the anti-SARS CoV-2 clinical interventions or have long been severe and transmissible but have vanished in the current scenario, hence don't pose any looming threat to the global public crowd.

COVID-19 is an alarming situation where the rise in the death toll and the mounting infection cases have called for a plausible therapeutic alternative competent against all the SARS-CoV-2 VoCs. To make the vision

of nullifying the pandemic more accurate, the focus has shifted from active immunization to passive immunization. In the era where passive immunotherapy, such as monoclonal antibody therapy, is trusted over other treatment options to curb the disease, the scalability for such a massive population is questionable in the long run. Despite these mAbs dominating medical interventions, they face issues penetrating the solid tissues, which limits their performance in a few diseases [3]. With significant effort, researchers have put forward an antibody mimic that imitates conventional antibodies and solves the manufacturing issue. The antibodies of these kinds are referred to as Nanobodies or VHH (Variable Heavy chain domains of Heavy-chain) antibodies derived from camelid immunoglobulin. These Nanobodies have the added advantage of being small, lacking the light chain, able to withstand high temperatures, easy scalability, and permit various modes of administration such as intranasal, intravenous injections, etc., and thus have the potential to substitute the monoclonal antibody. This class of single-chained antibody-Nanobody, has already paved its way in the FDA-approved drug library for the treatment of thrombocytopenic purpura and is commercialized under the name of Caplacizumab [4]. This has given an insight into designing Nanobody-based therapeutics utilizing anti-SARS-CoV-2 nanobodies for curbing the COVID-19 infection. The Receptor Binding Domain presents SARS-CoV-2 spike glycoprotein is the crucial part of the virus to dock against the hACE2 receptors to enter the host cell. This could be measured as the prime target for designing Nanobody-based therapeutics. Since the RBD is the chief hotspot for different mutations that give rise to the emergence of variants, it's important for a nanobody to bind the RBD of other VoCs to neutralize the circulating variants. Literature has already proven Nbs to tolerate the novel sprouting variants with a significant binding affinity and neutralization capability in many cell-based- and orthotropic animal models [5–7].

In a similar line, the present study was designed to demonstrate the rapidness of the advancing computational immunoinformatics in screening an already documented nanobody for constructing a biparatopic Nanobody-based antiviral against the viral spike RBD of the VoCs. Moreover, affinity maturation and PEGylation of the nanobody construct were accomplished to promote its therapeutic efficiency further. Subsequently, an antiviral peptide was introduced to block the hACE-2 receptor, ensuring a shield between the host and virus. Thereby, it would give an outline for making the class of Nbs a plausible alternative for subsisting anti-SARS-CoV-2 therapy, thus, proposing a precise treatment option for perspective pan-corona viruses (Fig. 1).

Methodology

Sequence and structure retrieval of SARS-CoV-2 VoCs RBD

To prevent any ambiguity in the data collection, a complete set of genomic sequences was picked for SARS-CoV-2 wild type and other SARS-CoV-2 VoCs, viz., Alpha (GISAID accession no. EPI_ISL_679974), Beta (GISAID accession no. EPI_ISL_2493065), Gamma (GISAID accession no. EPI_ISL_978506), Delta (GISAID accession no. EPI_ISL_1663516) and Omicron (BA.1, BA.2, BA.3) (GISAID accession no. EPI_ISL_6854348, EPI_ISL_8128463, EPI ISL 9,092,427) from the EpiCoVTM database coordinated by the Global Initiative on Sharing All Influenza Data (GISAID)(https://www.gisaid.org/) [1].

The amino acid sequence of SARS-CoV-2 wild-type (Wuhan-Hu-10) spike RBD was obtained from the NCBI database (https://www.ncbi.nlm.nih.gov/) (GenBank accession no.: NC_045512.2; PDB: 7OLZ_A) [8, 9]. The multiple sets of genomic sequences of the VoCs were subjected to ClusterOmega (https://www.ebi.ac.uk/Tools/msa/clustalo/) for multiple alignment to extract the sequence of the segment coding for the RBD in the spike glycoprotein in accordance with WT spike RBD, and visualized using Espript (Easy Sequencing in PostScript) server (https://espript.ibcp.fr/ESPript/cgi-bin/ESPript.cgi) server [10, 11]. Further, the identified RBD protein sequences analogous to SARS-CoV-2 VoCs were utilized for generating 3D models of VoCs RBD structures by the SWISS-MODEL server (https://swissmodel.expasy.org/interactive) [12]. SWISS-MODEL server is one of the most extensively used and cited tool for homology modelling of proteins as compared to other modelling tools to date. Later, the structure was refined using the GalaxyRefine2 tool (https://galaxy.seoklab.org/cgi-bin/submit.cgi?type=REFINE2) to advance the quality of the overall protein structure for downstream analysis [13].

Anti-SARS-CoV-2 nanobody library preparation and physiochemical profiling

The University of Oxford sponsors a publicly accessed Corona Virus Antibody Database, CoV-Abdab (http://opig.stats.ox.ac.uk/webapps/covabdab/), which gives a detailed account of all the drafted/patented neutralizing antibodies and nanobodies sampled against the SARS-CoV-2 wild type and other beta coronaviruses. As of April 21, 2022, the database shows 5,252 entries [14]. For the present study, amid a bunch of 636 nanobodies, we sorted

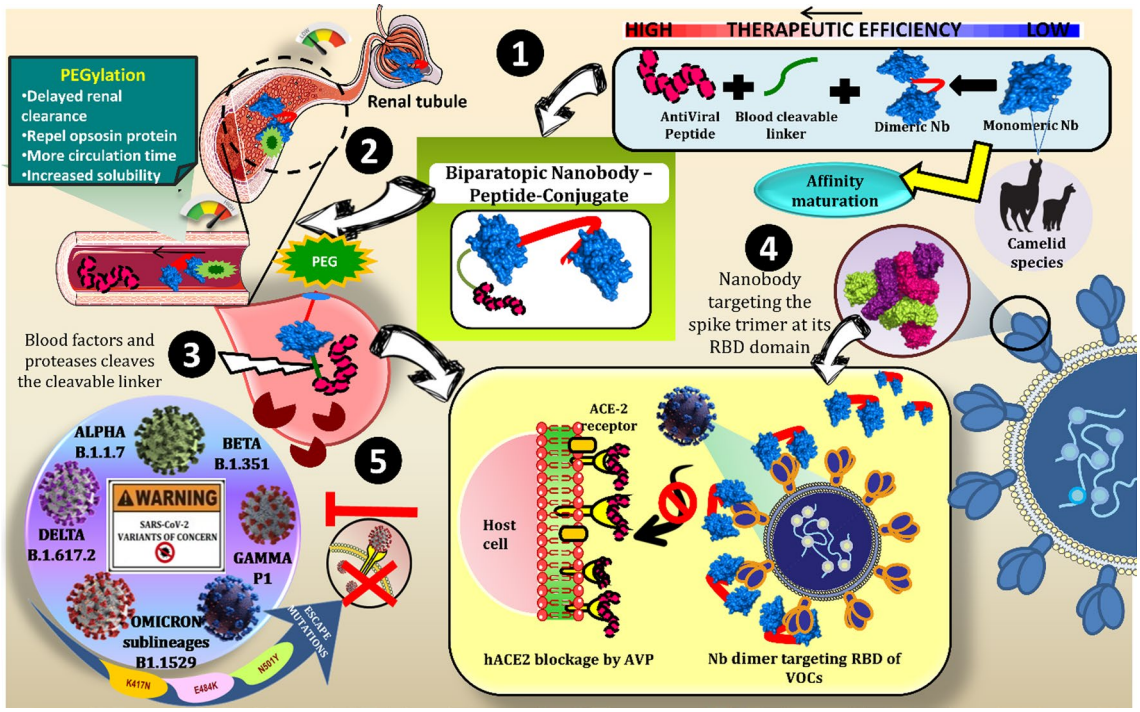

Fig. 1 Schematic illustration depicting the design of a biparatopic Nanobody Peptide Conjugate (NPC) to block the receptor binding domain of SARS-CoV-2 variants of concern with the hACE-2 receptor. (1) Construction of a biparatopic Nanobody-based antiviral by redesigning the monomeric nanobody by affinity maturation (by mutagenesis), multimerization (di-), and the insertion of an antiviral peptide that inhibits viral entry into the host cell to improve the therapeutic efficacy overall. (2) Modification of the biparatopic NPC by PEGylating it to increase its half-life, solubility and stability. (3) When the NPC encounters blood, proteases and blood factors split the blood cleavable linker into two distinct entities: a nanobody dimer and an antiviral peptide. (4) Nanobody binds to the spike glycoprotein's receptor binding region, effectively inhibiting the virus's major attachment point. (5) The antiviral peptide blocks the ACE2 receptor on the host cell's cellular surface, limiting viral penetration for all SARS-CoV-2 variants of concern (VoC)

nanobodies on the following criteria: (A) The nanobody must be able to target the SARS-CoV-2 spike RBD, (B) The Nanobody experimental crystal structure has been resolved, and could be mined from the Protein Data Bank, [15] (C) A nonrepetitive entry (D) No missing amino acid residue should be present in the Nb structure. The desired nanobody structures were scrutinized and extracted from the Protein Data Bank, followed by the PyMol visualization tool, and refined using the GalaxyRefine2 web interface [16, 17].

Later, we attempted to know the physiochemistry of the chosen Nanobodies, taking a brief account of different metrics such as molecular weight, pI, thermostability, hydrophobicity, solubility, and stability. First, the ExPASy-ProtParam tool (http://web.expasy.org/protparam/) was computed to obtain the molecular weight and pI for the Nbs, which was trailed by determining the thermostability of the Nbs by the SCooP web interface (http://babylone.ulb.ac.be/SCooP/) in terms of Tm (melting temperature). For stability and hydrophobicity prediction HLP server (http://crdd.osdd.net/raghava/hlp/help.html) was picked, and lastly, we assessed the solubility of the Nbs by the Protein sol server (http://protein-sol.manchester.ac.uk) [18–20].

Epitope mapping of conserved and mutable residues in VoCs RBD

With the rapid proliferation of variants, the odds of encountering novel escape mutations that can evade the host antibody-mediated response are also escalating. Thus, for an Nb to target both current and prospective circulating variants, it is critical to focus on the conserved residues in the spike RBD as a target. We used the ConSurf server (https://consurf.tau.ac.il/) to map significantly conserved epitopes in the spike RBD of distinct VoCs using site-specific conservation scores. It calculates the degree of conservation at each amino acid, with color codes ranging from cyan to purple marking the range of 0–9 from highly variable to extremely conserved regions [21]. Brief pathogenicity analysis was performed for the mutations undergone by the currently reported VoCs using a consensus web server known as PredictSNP (http://loschmidt.chemi.muni.cz/predictsnp) to pinpoint the deleterious and neutral mutations [22].

Molecular docking and assessment of energy variables

The panel of nanobodies was further described and analyzed for their ability to bind to the RBDs of interest for all the VoCs. However, before nanobody, and RBD docking, both the structures, i.e., Nbs and the VoCs RBD, are refined first using GalaxyRefine2, and the best-refined model with the highest RC plot values and RMSD (< 2 angstroms) was chosen as the optimized input files for docking [13]. Using the CLUSPRO 2.0 webtool (https://cluspro.bu.edu/login.php?redir=/home.php), each nanobody was docked against the RBD of SARS-CoV-2 (Wild type/Alpha/Beta/Gamma/Delta/OmicronBA.1/ BA.2/BA.3) utilizing its Antibody mode masking the non-CDR regions wherein the Nbs PDB was laid as receptor while the VoCs RBD as the ligand. The three computational steps used by the CLUSPRO server are rigid body docking using the fast Fourier transform (FFT) algorithm in billions of confirmations, clustering using the root mean square deviation of 1,000 of the lowest energy structures to classify the most likely model complex, and energy refinement of the overall complex structure. In FFT algorithm-based docking, the ligand (protein) is tethered on a moveable grid, while the receptor protein is placed at the origin of the coordinate system on a fixed grid. The binding energy terms are calculated, generating a scoring function. This helps the docking server produce structures that are more accurate and closely mirror native structures [23]. To predict the affinity with which Nbs bind with spike RBD, the top Nb-RBD model with the lowest binding energy of all the VoCs was sorted out. Then, their binding affinity was characterized by diverse benchmarking metrics to quantify the intermolecular strength in dissociation constants (Kd) and change in Gibbs free energy (ΔG) between the Nb-RBD complex. We dissected the ISLAND (In silico protein affinity predictor) (https://island.pythonanywhere.com/welcome/default/index#) server to access the binding affinity of the protein–protein complexes in terms of Kd and ΔG [24].

CDR delimitation and elucidation of contact residues in RBD-Nb complex.

The AbRSA web server (http://cao.labshare.cn/AbRSA/) was used to map the CDR regions regarded as the antigen-binding region of the given Nb. This server allows the numbering of the Nb and delimits the CDR region present in the molecule [25]. Later, the validation of individual CDR regions was executed using the IMGT/Collier-de-Perles tool (http://imgt.cines.fr), which permits a 2D graphical illustration of immune system proteins with color codes with a FASTA file as an input [26].

Further, the interacting residues for the best Nbs in the Nb-RBD complex were manually checked using PyMol and later validated in depth using LigPlot + extension DIMPLOT. PDBsum generates a schematic 2-D diagram for protein–protein interaction [27].

Molecular dynamics simulation of the best docked Nb

For the perceptive complex dynamics, we employed Simlab initiated WebGro (https://simlab.uams.edu/index.php) online server, in which we hired the best selected Nb with the RBD complexes of wild type and VoCs [28]. The complexes were simulated in 'Protein in water simulation' under online tools, and trajectory time was set to 20 ns with a temperature of 300 K to analyze the trajectories [29, 30].

Computational alanine scanning mutagenesis and docking studies with mutant Nb

To optimize the binding affinity of the Nb-RBD complex of each VoC, affinity maturation was performed by alanine scanning of the interacting site residues of the best-docked Nb. Drug Score PPI (https://cpclab.uni-duesseldorf.de/dsppi/) was utilized for computational alanine scanning of the Nb in the protein–protein interface of the Nb-RBD complex to identify the hotspot residues for mutagenesis [31]. The highest $\Delta\Delta G$ predicted free energy denoting the hotspots residues of Nb favorable for the mutation to Ala was then used for constructing a single mutant and subsequently multimutated library in all possible combinations via the PyMol Wizard mutagenesis tool. Then the mutant library was screened based on its binding affinity by docking the designed single, double, and triple mutants against the VoCs RBDs in round 1, round 2, and round 3 affinity maturation, respectively, through the HDOCK docking server (http://hdock.phys.hust.edu.cn/) [32]. The top-scoring mutant Nb docking against all the VoC's RBD was chosen for advancing workflow.

Screening of anti-viral peptide targeting hACE2 receptor

Spike glycoprotein's RBD domain interfaces with the ACE2 (EC number 3.4.17.23) receptor to allow it to enter the human body. This receptor must be considered the prime target to restrict SARS-CoV-2 from causing disease. We did this by screening an antiviral peptide library against the ACE2 receptor using the Antiviral Peptide Database (AVPdb) (http://crdd.osdd.net/servers/avpdb). The peptides having a role in inhibiting the viral entry were picked, which enumerate 650 peptides in the AVPdb library [33]. Various filters were employed to find the candidate peptide to sort the best AVP, such as length, allergenicity, antigenicity, toxicity, and physiochemical. Based on a few published

studies, the peptide length was fixed to 15 aa long. For the allergenicity of each AVP, the Algpred server (http://www.imtech.res.in/raghava/algpred/) was used then the antigenicity of the AVP was evaluated using the VaxiJen 2.0 server (http://www.ddgpharmfac.net/vaxijen) and the toxicity of the AVP was screened by ToxiNPred server (http://crdd.osdd.net/raghava/toxinpred/) [34–36]. For the physiochemical screening, first, the stability of the AVP was assessed using an HLP web server that gives the result in the form of half-life charge, pK, hydrophobicity, and charge [19]. Finally, the AVP's solubility was calculated using PepCalc.Com (https://pepcalc.com/peptide-solubility-calculator.php) computational server [37].

Before attaching AVP to the Nb, it is vital to confirm the attachment of AVP to the ACE2 receptor. Based on numerous published studies, it is shown that the ACE2 interacts with the spike RBD hotspots via interacting residues, viz. Ser19, Gln24, Tyr83, Lys31, Glu35, His34, Asp38, Glu37, Tyr41, and Lys353. To achieve this, we did a site-specific docking using the HDOCK server (http://hdock.phys.hust.edu.cn/), where we docked the top physiochemical screened AVP with ACE2 by specifying the interacting residues sites. The best-docked AVP with the lowest binding energy was selected for subsequent studies [32].

Nanobody dimerization and structural assembly with antiviral peptide

Multimerization/multivalent format of Camelid-derived Nanobodies has been widely documented to improve the binding affinity and thus neutralizing potency against SARS-CoV-2, as per available literature [38]. With this in mind, a homodimer of chosen Nb was constructed, linking the two entities of Nb with $(GGGGS)_3$ flexible linker and subsequently evaluating its binding affinity with the VoCs RBD using HDOCK. This was followed by adding the singled-out anti-viral peptide to the non-CDR portion of the dimer. To ensure the attachment of the best-docked AVP, it is essential to tie the peptide with a blood-cleavable linker. Next to cleavage, two fused proteins/peptides are detached to function independently. Chen et al. designed an *in-vivo* cleavable disulfide (LEAGCKNFFPRSFTSCGSLE) that was created using a dithiocyclopeptide with an intramolecular disulfide bond formed between two cysteines (Cys) residues on the linker and a thrombin-sensitive sequence (PRS) between both the Cys residues [39]. We used this linker to fuse nanobodies with the AVP, which could later separate at their site of action. We also used the PROSPER (http://lightning.med.monash.edu.au/PROSPER/) and PeptideCutter (https://web.expasy.org/cgi-bin/peptide_cutter/peptidecutter.pl) server to locate the protease targeting cleavable sites of Dithiocyclopeptide [40, 41]. We assembled the dimer Nb, linker, and the finalized AVP using the I-TASSER server (https://zhanggroup.org/I-TASSER/) to generate a full-length 3D conjugated Biparatopic Nb model prediction in the PDB format. The model selection was based on benchmarked scoring systems such as the confidence score, estimated TM score and RMSD to quantitatively evaluate the quality of the I-TASSER model [42]. To validate the correctness of the final construct, the ProSA web server of the 3D model and SWISS Model located the constructs residue in the Ramachandran plot. Lastly, the flexibility of the NPC was determined by simulating the structure in CABSFlex server [43–45].

Physiochemistry, toxicity & pegylation of biparatopic nanobody-peptide-conjugate

The final biparatopic Nb-peptide-conjugate was evaluated on physiochemical grounds, including solubility, thermostability, and molecular weight calculated using the previously used Protein sol, SCooP, and ExPaSy server, respectively. In contrast, toxicological parameters were checked using ToxiNPred, Algpred, and VaxiJen 2.0 in the order of toxicity, allergenicity, and antigenicity [18, 20, 34–36, 46].

In general, small-sized Nb-conjugate is susceptible to rapid renal clearance. To reimburse this constraint, studies have evidenced the Nb format's PEGylation -PEG (EC Number 500-038-2) that has ultimately improved its solubility, reduced immunogenicity, prevented proteolysis, and permitted retention time that allows low-dosing frequency [47]. Hence, PEGylation was carried out by attaching 20 kDa linear maleimide (EC Number: 208-787-4) -terminated PEG (MAL-$(PEG)_n$-OMe) to the Cysteine residue at the N terminal of one of the Nb.

Codon optimization and in-silico cloning

Codon optimization and reverse translational to Nb coding sequence were carried out with the goal of cloning and in silico engineering, the final Biparatopic nanobody constructs in the eukaryotic yeast-surface display expression vector. The protein sequence of the nanobody construct was used as the input sequence in the VectorBuilder tool (https://en.vectorbuilder.com/tool/codon-optimization.html). To ensure a high expression rate, the host organism was chosen as a Human (Homo sapiens) cell line, and the sites for two restriction enzymes, Acc65I and XbaI, were blocked. For the query Nb construct, the server returns a cDNA output along with parameters such as codon adaptive index (CAI) and GC content for the protein sequence. The availability of any commercially available restriction cleavage sites for the GOI was checked using NEBcutter [48]. The restriction sites Acc65I and XbaI were then introduced to the N- and C-terminal ends, respectively. We used the SnapGene restriction cloning software (www.snapgene.com) to clone

the Nb construct GOI into yeast, specifically the *Pichia pastoris* expression vector Ppicza, which has proven to yield 6-13.6 times greater expression than *E.coli* without any glycosylation sites detected [49].

Results

Homology modelling and structural refinement of VoCs RBD

Since RBD is the primary site of contact between the viral pathogen and the host, to generate the RBD models of individual VoCs and the wild type of SARS-CoV-2, the FASTA sequences were obtained from GISAID and NCBI, respectively. All the sequences were subjected to multiple sequence alignment concerning the WT RBD, whose output was visualized using ESPript. SWISS-MODEL generated homology models for RBD of each described variant using the extracted RBD sequences from different alignments pinpointing the highlighted mutant residues. GalaxyRefine2 optimization was applied to the best models with (> 90%) RC favorable, moderately substantial QMEAN and GMQE, and the highest sequence identity. Further to the generated models, the model with criteria, i.e., low RMSD (> 2 angstrom) and (> 95%) RC favorable was chosen, which ensured that the computational pipeline we applied for model generation shows minimum deviation from the experimentally determined models and reliable for advancing steps.

Physiochemical screening of SARS-CoV-2 neutralizing Nbs

Our analysis from the CoV-Abdab database targeting the SARS-CoV-2 WT and VoCs obtained 636 Nbs, of which 45 Nbs had experimentally derived crystallized PDB structures (Supplementary Table 1). Using PyMol, Nb 3D models was extracted followed by structure refinement using GalaxyRefine2. For the refined models, we chose the models with low RMSD (> 2 angstroms) and high RC fair values. The preliminary screening of the Nb based on various physicochemical properties like molecular weight and pI were calculated using ExPasy-Protparam, which deduced the Nbs molecular weight ranging from 13.5 to 15 kDa (unlike mAbs ~ 150 kDa) (Fig. 2a), and pI ranging 4.7–9.4 where the majority of the Nbs had 8–9 pI which is considered adequate therapeutic Nbs administration (Fig. 2b). Nb is known to show thermoresistance, and the Tm value measured from

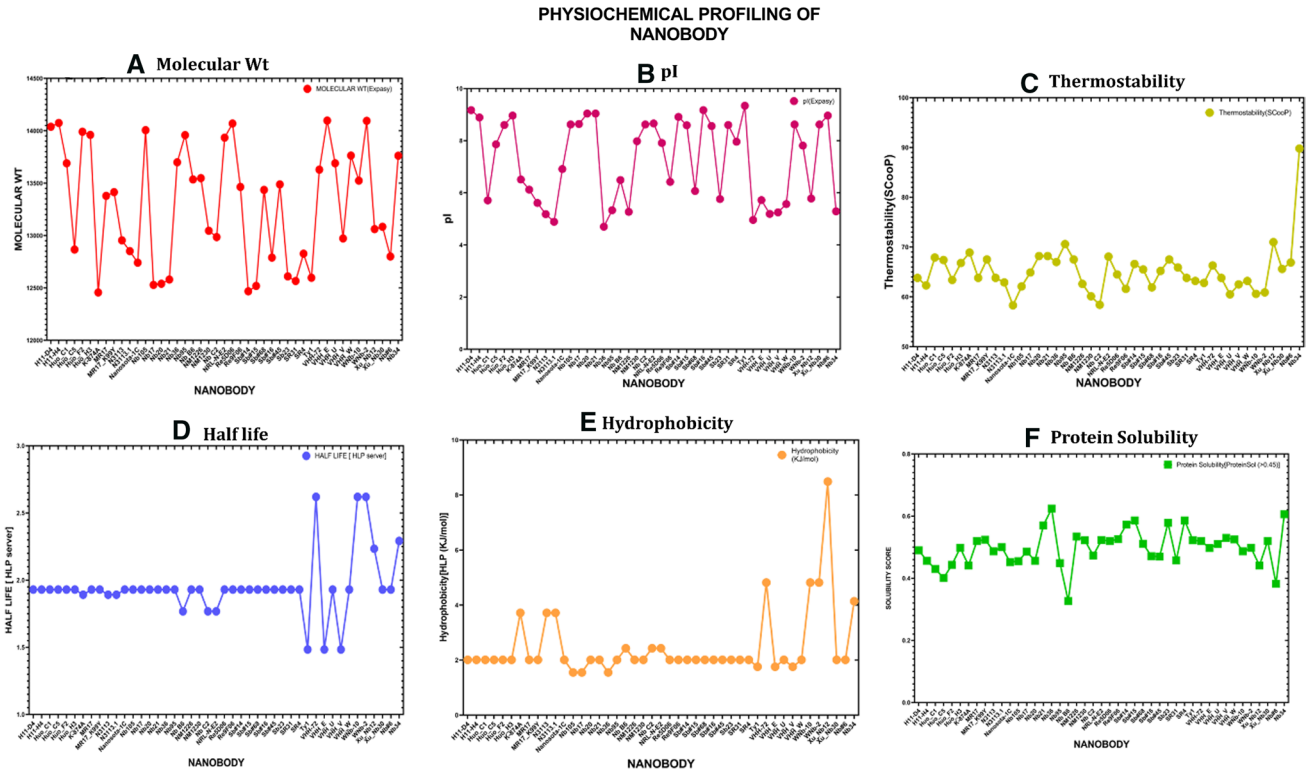

Fig. 2 Physiochemical attributes of the Nanobodies. **a** Molecular weight and **b** pI obtained from ExPasy Protparam server. **c** Thermostability calculated from the SCooP server. **d** Half-life and **e** hydrophobicity estimated by the HLP server. Lastly, **f** Protein solubility measured using the ProteinSol server (> 0.45 score considered to be soluble). The data for the physiochemical profiles of the nanobody was visualized using GraphPad Prism v.9 software

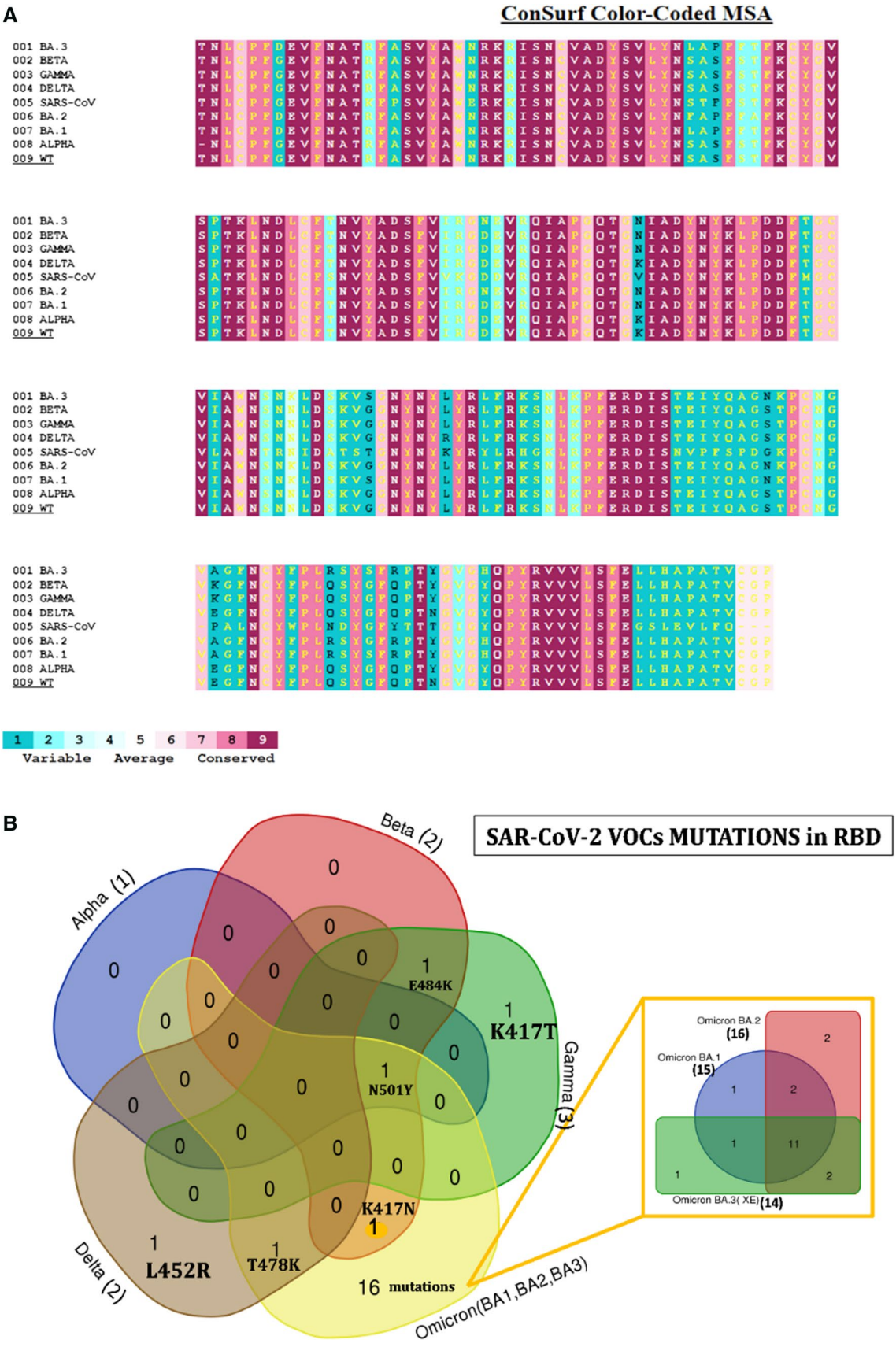
A
ConSurf Color-Coded MSA
001 BA.3
002 BETA
003 GAMMA
004 DELTA
005 SARS-CoV
006 BA.2
007 BA.1
008 ALPHA
009 WT
1 2 3 4 5 6 7 8 9
Variable Average Conserved
B
SAR-CoV-2 VOCs MUTATIONS in RBD
Alpha (1)
Beta (2)
Gamma (3)
Delta (2)
Omicron(BA1,BA2,BA3)
E484K
K417T
N501Y
K417N
L452R
T478K
16 mutations
Omicron BA.2 (16)
Omicron BA.1 (15)
Omicron BA.3(XE)(14)

◂**Fig. 3** Epitope mapping of conserved residues and pathogenicity analysis. **a** Consurf prediction of conserved spike RBD epitopes of SARS-CoV-2 VoCs colored coded based on their conservation scores where the color cyan represents low scores representing highly mutable/variable residues and the color purple with high scores portray highly conserved residues in the cyan through purple color bar. **b** A Schematic Venn diagram (obtained using http://bioinformatics.psb.ugent.be/webtools/Venn/) illustrating shared mutations between SARS-CoV-2 variants of concern

the SCooP webserver denoted the 45 Nbs to have Tm in the range of 55–70°, which shows agreement with this notion (Fig. 2c). The half-life measured in seconds establishes the peptide stability in direct relation to the half-life, i.e., the higher half-life greater the peptide stability (Fig. 2d) and hydrophobicity (Fig. 2e), where the HLP tool showed harmony with the high stability of all the 45 Nbs. Solubility assessment of Nbs pays equal importance rendering to its clinical application. Protein sol predicted 40 out of 45 Nbs to have high water solubility featured on the table (Fig. 2f). To screen the panel of Nbs further, a comparison was made based on its binding affinity described in the upcoming sections.

Identification of conserved and mutable epitopes of VoC's RBD

The ConSurf server estimated the evolutionary rate of the amino acid epitopes of the spike RBD of each VOC. The color schemed purple region depicts the highly conserved residues of individual RBDs. The MSA results and the conservation scores are summarized in the figure (Fig. 3a). Briefly scrutinizing the pieces of literature and WHO profiles, reported the mutations sustained by the spike RBD of VoCs,- Alpha (N501Y); Beta (K417N, E484K, N501Y); Gamma (K417T, E484K, N501Y); Delta (L452R, T478K); Omicron BA.1 (G339D, S371L, S373P, S375F, K417N, N440K, G446S, S477N, T478K, E484A, Q493R, G496S, Q498R, N501Y, Y505H); Omicron BA.2 (G339D, S371F, S373P, S375F, T376A, D405N, R408S, K417N, N440K, S477N, T478K, E484A, Q493R, Q498R, N501Y,Y505H), and Omicron BA.3 (G339D, S371L, S373P, S375F, D405N, N440K, G446S, S477N, T478K, E484A, Q493R, Q498R, N501Y, Y505H). The shared mutations in these VoCs are represented in the Venn diagram (Fig. 3b).

Among them, the mutations N501Y, L452R, and Y505H were predicted to be deleterious, and the rest of the mutations had neutral effects regarding pathogenicity. At the same time, few servers have shown the mutations G496S in BA.1 and T376A in BA.2 to be disease-causing. All the VoCs share the mutation N501Y, and the mutation L452R is responsible for the pathogenic behavior of the Delta variant. The final table was prepared by taking the results from highly reliable PredictSNP with percentages denoting the accuracy of prediction along with the overall extended results from all the six servers (PredictSNP, PolyPhen1, PolyPhen-2, SIFT, SNAP, PANTHER. The pathogenicity was established based on a manually designed confidence score defining the likelihood of a mutation deleterious (Table 1).

Molecular docking analysis of Nbs-VoCs RBD complex and evaluation of binding affinity

The preoptimized homology-modeled PDB structures were chosen relying on MolProbity scores (lower MolProbity value, more the mechanically realistic model) and lower RMSD scores; they were subjected to protein–protein molecular docking. CLUSPRO docking server was operated for docking the pane of 45 Nbs with RBDs of WT and individual VoCs. The best 9 Nbs-RBD model with the lowest binding energy showing significant interaction between Nbs and RBD epitopes was preferred for further analysis. The Nbs Re5D06 (PDB:7OLZ), WNb-2 (PDB:7LDJ), MR17_K99Y (PDB:7CAN), N3113 (PDB:7VNB), N3113.1 (PDB:7VNE), VHH_W (PDB:7KN7), Nb36 (PDB:7MEJ), WNb-10 (PDB:7LX5), Sb23 (PDB:7A25), and NRL-N-E2 (PDB:7N0I) exhibited effective binding with the RBD of VoCs with binding energy scores mostly above -290 kcal which could be graphically examined by the heat map at (Fig. 4a) [5, 9, 50–55]. Taking the wild-type RBD as the control, the binding energy for Nbs VHH_W, Nb36, MR17_K99Y, WNb-2, Re5D06, N3113 complexed with the VoCs RBD had increased binding energy for all or majority of the RBDs. It can also be noted that the Nb VHH_W, MR17_K99Y, and Nb 36 showed remarkably stronger binding affinity to the RBD of the Omicron sub-lineages. We also observed that despite the Nb Re5D06 having improved affinity towards the Omicron RBD, the trend reduced for other VoCs RBD such as Alpha, Beta, and Gamma. For a nominee Nb, we were interested in selecting the Nb having ample affinity towards all the existing VoCs for further analysis. Their greater binding effectiveness, evidenced by their docking score, suggests that they could be used in mutational investigations to develop a more efficient antiviral nanobody.

Computational techniques may generate multiple criteria for predicting binding affinity in protein–protein complexes, and mispredictions may affect the accuracy of future analysis and interpretations. We took the predicted dissociation constant (Kd) and change in Gibbs free energy (ΔG), denoting the binding affinity point of reference against the Nb-RBD complexes. Many studies have suggested the inverse relationship between Kd and binding affinity, where smaller Kd depicts stronger binding affinity and vice versa. Usually, for an antibody-like molecule (Nb in the present context), the Kd ranges

Table 1 Pathogenicity estimation of Spike RBD substitutions (mutation) using PredictSNP server

S. no.	SARS-CoV-2 VOCs	MUTATIONS(WHO)	PredictSNP	Predicted type	Overall Pathogenicity Confidence score (PredictSNP, PolyPhen1, PolyPhen-2, SIFT, SNAP, PANTHER) (%)	Predicted type
1	ALPHA	N501Y	0.63	Neutral	33.34	Neutral
2	BETA	K417N	0.83	Neutral	0.00	Neutral
		E484K	0.83	Neutral	0.00	Neutral
		N501Y	0.51	Deleterious	66.67	Deleterious
3	GAMMA	K417T	0.83	Neutral	0.00	Neutral
		E484K	0.83	Neutral	0.00	Neutral
		N501Y	0.51	Deleterious	66.67	Deleterious
4	DELTA	L452R	0.52	Deleterious	66.67	Deleterious
		T478K	0.83	Neutral	0.00	Neutral
5	OMICRON (BA.1)	G339D	0.83	Neutral	0.00	Neutral
		S371F	0.79	Deleterious	100	Deleterious
		S373P	0.63	Neutral	33.34	Neutral
		S375F	0.63	Neutral	33.34	Neutral
		K417N	0.65	Neutral	33.34	Neutral
		N440K	0.74	Neutral	33.34	Neutral
		G446S	0.55	Neutral	33.34	Neutral
		S477N	0.63	Neutral	33.34	Neutral
		T478K	0.83	Neutral	0.00	Neutral
		E484A	0.6	Neutral	50.00	Possibly deleterious
		Q493R	0.75	Neutral	16.67	Neutral
		G496S	0.55	Deleterious	83.34	Deleterious
		Q498R	0.63	Neutral	33.34	Neutral
		N501Y	0.63	Deleterious	66.67	Deleterious
		Y505H	0.87	Deleterious	100	Deleterious
6	OMICRON (BA.2)	G339D	0.83	Neutral	0	Neutral
		S371F	0.79	Deleterious	100	Deleterious
		S373P	0.63	Neutral	33.34	Neutral
		S375F	0.63	Neutral	33.34	Neutral
		T376A	0.55	Deleterious	83	Deleterious
		D405N	0.52	Deleterious	83	Deleterious
		R408S	0.6	Neutral	50	Possibly deleterious
		K417N	0.65	Neutral	33.34	Neutral
		N440K	0.74	Neutral	16.67	Neutral
		S477N	0.63	Neutral	33.34	Neutral
		T478K	0.83	Neutral	0	Neutral
		E484A	0.6	Neutral	50	Possibly deleterious
		Q493R	0.75	Neutral	16.67	Neutral
		Q498R	0.63	Neutral	33.34	Neutral
		N501Y	0.63	Neutral	33.34	Neutral
		Y505H	0.87	Deleterious	100	Deleterious

Table 1 (continued)

S. no.	SARS-CoV-2 VOCs	MUTATIONS(WHO)	PredictSNP	Predicted type	Overall Pathogenicity Confidence score (PredictSNP, PolyPhen1, PolyPhen-2, SIFT, SNAP, PANTHER) (%)	Predicted type
7	OMICRON XE (BA.3) [Stealth]	G339D	0.83	Neutral	0	Neutral
		S371L	0.61	Neutral	33.34	Neutral
		S373P	0.63	Neutral	33.34	Neutral
		S375F	0.63	Neutral	33.34	Neutral
		D405N	0.52	Deleterious	83	Deleterious
		N440K	0.74	Neutral	16.67	Neutral
		G446S	0.65	Neutral	33.34	Neutral
		S477N	0.63	Neutral	33.34	Neutral
		T478K	0.83	Neutral	0	Neutral
		E484A	0.6	Neutral	50	Possibly deleterious
		Q493R	0.75	Neutral	16.67	Neutral
		Q498R	0.63	Neutral	33.33	Neutral
		N501Y	0.63	Neutral	33.33	Neutral
		Y505H	0.87	Deleterious	100	Deleterious

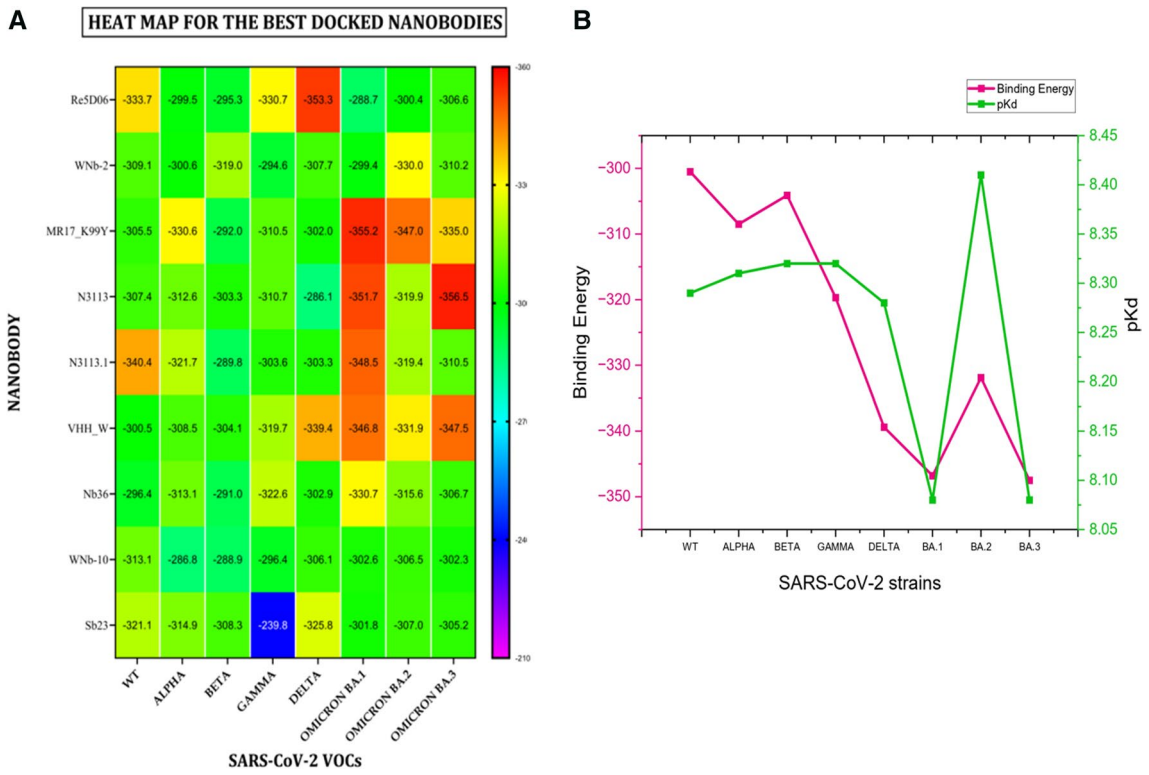

Fig. 4 Analyzing Nb-RBD docking results **a** Heatmap representing the CLUSPRO generated binding energy for best docked Nbs made using GraphPrism. **b** The line plot diagram for the Nb VHH W highlights its binding energy and picomolar affinity in terms of pKd against all the SARS-CoV-2 variants of concern

from 10^{-6} to 10^{-9}. The ΔG is a scoring function giving a vague idea about the extent to which the docking pose is favorable for interaction. According to the results of the ISLAND server, the binding affinity of the Nbs such as VHH_W, MR17_K99Y, and WNb-10 have shown increased binding affinity with the majority of SARS-CoV-2 VoCs RBDs. We took the wild type or Wuhan-Hu-1 strain as the reference interaction.

For designing a clinically relevant drug candidate, binding affinity holds considerable importance, attributed to its specificity, selectivity, and neutralization activity. Kd in the picomolar range is accounted significant in catering to the antigen–antibody interaction and could be subjected as a high-affinity Nb fragment, which amplifies the interactions to various folds. ISLAND server-driven output channelized the workflow towards sorting an Nb binding all the VoCs RBD, and thus we sized our study on Nb VHH W having a picomolar ranged binding affinity with all the VoCs strains [56]. Figure shows the graphical representation of binding energy and pKd (calculated by taking the log of Kd) of Nb VHH W (Table 2, Fig. 4b).

Contacting residues at the RBD-Nb interface and their propensity with Nb CDRs

To map the hypervariable-CDR loops of the nanobody VHH W, the preliminary analysis was made by the AbRSA tool in IMGT antibody (nanobody) numbering. Subsequent validation was achieved for the delimitation made by IMGT/*Colliers de Perles* that uses the Nb VHH W FASTA to highlight the CDR1, CDR2, and CDR3 loops of the nanobody governing the key antigen recognition role (Fig. 5).

SARS-CoV-2 variants include myriads of RBD mutations that impair mAb or Nb binding, underscoring the need for antivirals resistant to viral escape. To ensure a robust binding affinity against all the VoCs included in the study, we identified the cryptic epitopes of RBD directing the interactions with Nb CDR. To assess the extent to which the presented Nb VHH W shows competence to target the critical conserved site and block the existing reported mutations in RBD of VoCs by the competitive inhibition with hACE-2, a meticulous analysis of the interacting residue performed at residue level manually for Nb VHHW-RBDs complexes with the PyMol visualization tool. Further particular focus was made on the contacting residues of the Nb VHH W-RBD complex involving CDR regions of the Nb and the

Table 2 Binding affinity of the Nbs-RBD complex calculated in terms of Kd and ΔG using ISLAND server

S. no.	Nanobody	Wild type		Alpha		Beta		Gamma	
		Kd (M) at 25.0 ℃	ΔG (kcal mol−1)	Kd (M) at 25.0 ℃	ΔG (kcal mol−1)	Kd (M) at 25.0 ℃	ΔG (kcal mol−1)	Kd (M) at 25.0 ℃	ΔG (kcal mol−1)
1	Re5D06	4.80E−09	− 11.33	9.85E−09	− 11.31	5.0423–09	− 10.91	9.85E−09	− 10.91
2	WNb-2	7.50E−09	− 11.07	7.30E−09	− 11.09	7.23E−09	− 11.10	7.24E−09	− 11.10
3	MR17_K99Y	8.25E−09	− 11.02	7.96E−09	− 11.04	7.89E−09	− 11.05	7.89E−09	− 11.04
4	N3113	2.68E−09	− 11.68	2.74E−09	− 11.67	2.60E−09	− 11.69	2.68E−09	− 11.70
5	N3113.1	2.95E−09	− 11.63	3.02E−09	− 11.61	2.91E−09	− 11.64	2.90E−09	− 11.64
6	VHH_W	5.03E−09	− 11.31	4.84E−09	− 11.33	4.80E−09	− 11.34	4.80–09	− 11.34
7	Nb36	1.30E−08	− 10.71	1.35E−08	− 10.73	1.33E−08	− 10.73	1.33E−08	− 10.73
8	WNb-10	4.80E−07	− 11.34	4.93E−09	− 11.32	4.75E−09	− 11.35	4.75E−09	− 11.34
9	Sb23	2.61E−09	− 11.70	2.67E−09	− 11.68	2.57E−09	−11.71	2.57E−09	− 11.71
S. no.	Nanobody	Delta		Omicron (BA.1)		Omicron (BA.2)		Omicron (XE)	
		Kd (M) at 25.0 ℃	ΔG (kcal mol−1)	Kd (M) at 25.0 ℃	ΔG (kcal mol−1)	Kd (M) at 25.0 ℃	ΔG (kcal mol−1)	Kd (M) at 25.0 ℃	ΔG (kcal mol−1)
1	Re5D06	9.85E−09	− 10.91	1.37E−08	− 10.72	4.27E−09	− 11.41	1.24E−08	− 10.78
2	WNb-2	6.85E−09	− 11.13	1.25E−08	− 10.77	6.98E−09	− 11.12	1.20E−08	− 10.80
3	MR17_K99Y	7.41E−09	− 11.08	1.39E−08	− 10.71	4.89E−09	− 11.33	1.18E−08	− 10.81
4	N3113	2.82E−09	− 11.65	2.83E−09	− 11.65	3.24E−09	− 11.57	1.00E−08	− 10.90
5	N3113.1	3.10E−09	− 11.60	3.11E−09	− 11.59	3.55E−09	− 11.52	1.11E−08	− 10.84
6	VHH_W	5.18E−09	− 11.29	8.30E−09	− 11.01	3.86E−09	− 11.47	8.01E−09	− 11.04
7	Nb36	1.20E−08	− 10.79	2.26E−08	− 10.42	6.40E−09	− 11.17	1.19E−08	− 10.80
8	WNb-10	3.39E−09	− 11.55	5.02E−09	− 11.31	5.71E−09	− 11.24	1.35E−08	− 10.73
9	Sb23	2.75E−09	− 11.67	2.76E−09	− 11.67	3.15E−09	− 11.59	1.90E−08	− 10.71

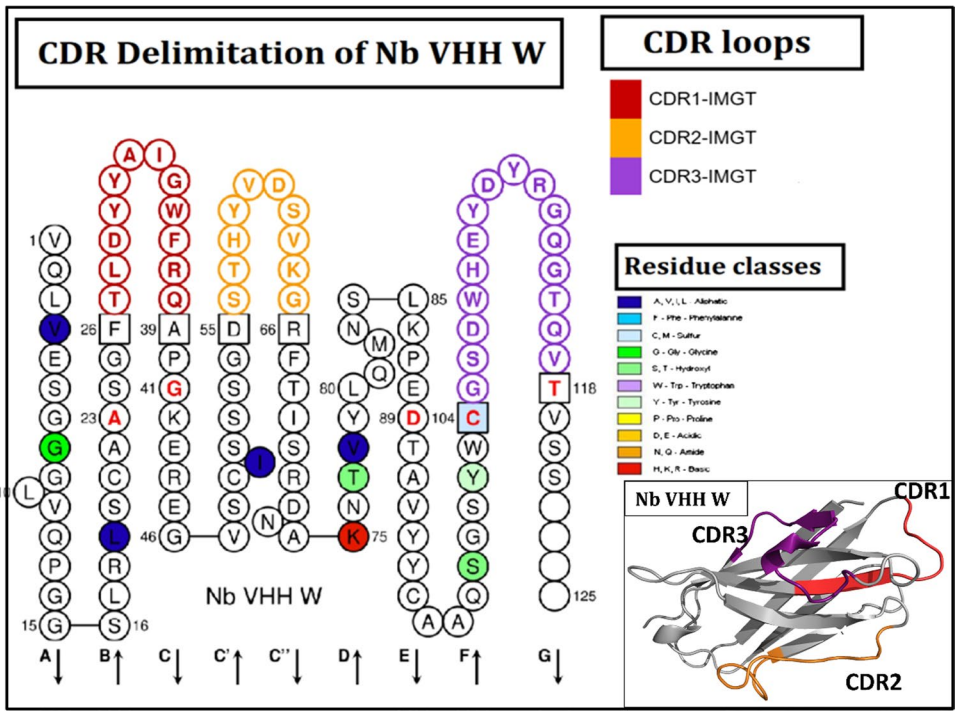

Fig. 5 CDR delimitation of Nb VHH W in IMGT numbering featuring the three CDRs anchoring loops where maroon color shows the CDR 1 loop, orange color shows CDR 2 and purple shows the CDR 3 region residues obtained using IMGT/*Colliers de Perles* platform

conserved RBD epitopes at the interface. Since deleterious mutations have been known to subdue the binding affinity of Nb, the CDR paratopes of the Nb binding with neutral (non-deleterious) mutations (and RBD hotspot residues) could be counted as effective in barricading the communication of RBD to ACE-2 in the existing VoCs (Fig. 6).

Critical analysis of RBD-Nb interacting residues

When it comes to processing an Nb-based drug candidate, the Nb VHH-W might be thought of as the one with an affinity for all variations and many residue interactions in its CDR for conjugate drug creation. Nb VHHW CDR3 loop encompasses residues 104 to 118, CDR2 loop 55to 66, and CDR1 loop 26 to 39. A comprehensive investigation of the contacting interface residues in the Nb-RBD complex was performed using Dimplot + extension of Ligplot + and PDB-sum produced diagrams.

VHH W-WT RBD

Scrutinizing the interactions of VHH W with the wild-type SARS-CoV-2, out of a total of 9 interacting residues of VHH W, we found that it could simply employ 8 of its residues from the CDR3 and CDR1 region for interaction with Wild type RBD. Four CDR3 residues and one CDR1 bind to the highly conserved residues of WT RBD as Arg114/ARG 457, Glu110/Gln409, Asp112/Tyr421, Tyr113/Thr415; and Gln38/Tyr489, respectively, with Consurf conservation score of 8–9 indicating highly conserved residue (Fig. 6a).

VHH W-ALPHA RBD

Briefing on the interaction between Nb VHH W with the RBD of Alpha type, with the interaction of 9 Nb residues of which four CDR3 residues and two CDR1 residues participate as contacting residue. The CDR3-RBD contacting residues involving conserved epitopes present in the purple region depicting conserved residue of RBD are constituted as (CDR3 Nb residues/conserved RBD residues) Glu110/Gln409. At the same time, the CDR1 interaction goes as Phe26/Tyr 489, and Thr 27/Asn 487 (Fig. 6b).

VHH W-BETA RBD

Observations were then made in the case of Nb-beta RBD, where the 9 Nb VHH W contacting residue protruded its CDR arms. None of the interactions found included the non-CDR region. The CDR region of VHH W Beta RBD had interactions as (CDR3 Nb residues/conserved RBD residues) Tyr111/Cys 480; and (CDR1 Nb residues conserved RBD) Asp29/Ile468. The conserved RBD residues targeted by the Nb CDR indicate the prospective effect of the neutralizing Nb even in the case of any RBD mutations in the upcoming variants (Fig. 6c).

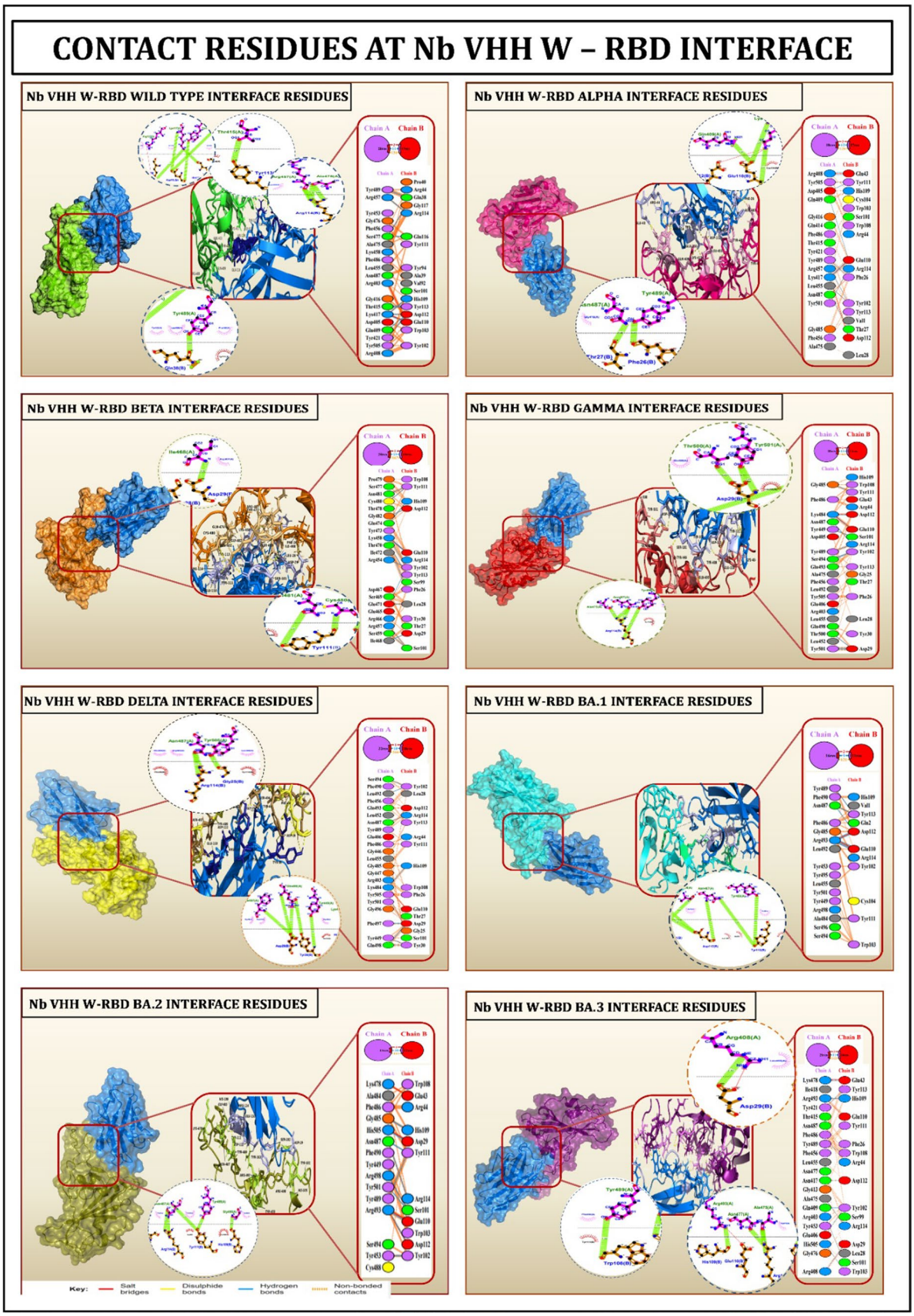
CONTACT RESIDUES AT Nb VHH W – RBD INTERFACE
Nb VHH W-RBD WILD TYPE INTERFACE RESIDUES
Nb VHH W-RBD ALPHA INTERFACE RESIDUES
Nb VHH W-RBD BETA INTERFACE RESIDUES
Nb VHH W-RBD GAMMA INTERFACE RESIDUES
Nb VHH W-RBD DELTA INTERFACE RESIDUES
Nb VHH W-RBD BA.1 INTERFACE RESIDUES
Nb VHH W-RBD BA.2 INTERFACE RESIDUES
Nb VHH W-RBD BA.3 INTERFACE RESIDUES
Chain A
Chain B
Key:
Salt bridges
Disulphide bonds
Hydrogen bonds
Non-bonded contacts

◂**Fig. 6** Interacting residues at the Nanobody VHH W- RBD interface in SARS-CoV-2 VoCs. The surface depiction of Nanobody VHH W (Blue) in complex with **a** Wild type (Green), **b** Alpha variant (Pink), **c** Beta variant (Orange), **d** Gamma variant (Red), **e** Delta variant (Yellow), **f** Omicron BA.1 (Cyan), **g** Omicron BA.2 (Olive), **h** Omicron BA.3 (Violet). The close-up stick diagram of the interacting amino acids of complexes is a result of molecular docking performed using CLUSPRO server and visualized in PyMol. The 2D Ligplot + extension Dimplot diagram within the circular boxes highlights the conserved RBD residues interacting with the CDR loops of the Nb VHH W where the green line indicates the hydrogen bonds. The pictorial illustration extracted from PDBsum server shows all the interface contacting residues between Chain A (RBD) and Chain B (Nb VHH W) where the blue line represents H bond, yellow represents the disulfide bond, red line represents the hydrophobic interaction and dotted orange line shows the nonbonded residues. (The reader is directed to the Web version of this article for an explanation of the colour references in this figure legend)

VHH W-GAMMA RBD

The Gamma variant's RBD is targeted by 7 Nb VHH W residues where the CDR3 region project one residue to RBDArg114/Asn487-Tyr489, but CDR1 binds as Asp29/Thr500which are found evolutionarily conserved (Fig. 6d).

VHH W-DELTA RBD

A sum of 7 interacting amino acids of Nb VHH W forms a bond with the Delta strains. Of which, three conserved RBD residues attach to Nb CDR3 paratope as Arg114/Asn487, and CDR1 interact through Tyr30/Tyr 449 (Fig. 6e).

VHH W-OMICRON BA.1 RBD

For the unprecedented mutation-prone Omicron variant (BA.1), the chosen Nb VHH W displayed affinity through CDR3 and framework region only. Structurally, there are 4 Nb residues utilizing its CDR3 to bind with RBD- Asp112/Asn487, Tyr 113/Tyr 489. In addition, this Nb perfectly targets the existing mutations where the Nb VHH W could compete with the hACE2 for binding to the RBD (Fig. 6f).

VHH W-omicron BA.2 RBD

Only three CDR3 residues were able to bind the RBD non-mutable epitopes in the latest Omicron BA.2 subvariant, out of a total of nine Nb VHH W paratopes involved: Arg114/Asn487, Tyr111/Ty489, and His109/Gly485. The inclusion of the mutation N501Y culminates in a sevenfold greater binding affinity to the hACE2 receptor as compared to the original wild-type SARS-CoV-2 virus. The Tyr mentioned above mutation produces considerable virulence in highly transmissible Omicron variants. In the current context, the selected Nb VHH W might considerably bind and restrict the N501Y via Ser 101, a framework region derivative. This means that by undergoing competitive inhibition, it can potentially limit Omicron BA.2 variant invasion by halting attachment to the central hACE2 receptor. We could also speculate that CDR3 restricts the hACE2 binding hotspot present in RBD(Tyr 489) with the help of Tyr111. As a result, this Nb would be able to negate any existing BA.2 subvariants. On the other hand, several residues target RBD's conserved residues, providing the Nb a futuristic edge (Fig. 6g).

VHH W-omicron BA.3 RBD

Ultimately, the recently identified recombinant stealth variant termed XE (BA.3) subvariant has mutations from both BA.1 and BA.2 and can bind a maximum of conserved XE RBD epitopes. The Nb interface extends 12 residues to address the XE RBD. Out of which nine residues belong to the CDR3 region, one belongs to the CDR1 region explicitly targeting the conserved RBD residues, i.e., Trp108/Tyr489, His109/Arg493, Arg114/Ala475-Asn477, Tyr113/Tyr421; and Asp29/Arg408 respectively (Fig. 6h).

It's worth noting that Lys 484 is one of the WHO-reported mutations in Gamma and Delta SARS-CoV-2 variants, which has been linked to immunological invasion, which amplifies the interaction between ACE2 and RBD by a factor of ten. The Nb VHH W paratopes Glu110 in Gamma and His109 and Glu110 in Delta may block the Lys 484 from additional contact with the host receptor and other coreceptors involved with increased infectivity.

As per what we know about the Tyr 501 (Y501) mutation, from literature review and PredictSNP results, which is prevalent in Alpha, Beta, Gamma, and Omicron forms, it is liable for more significant interaction between RBD and ACE2. Tian et al. and coauthors employed FACS assays, surface plasmon resonance, and molecular dynamics to establish the more arduous interaction in RBD caused by the N501Y mutation, leading to increased transmissibility in SARS-CoV-2 VoCs [57]. Taken together, we might speculate that the Nb VHHW can effectively impede the binding residue Tyr501, reducing the likelihood of an RBD-hACE2 complex forming.

Kumar et al., attempted to conduct a pathogenicity analysis and resolve the electrostatic surface potential of spike glycoprotein, which established that among the many Omicron mutations, one of the mutations, i.e., His505 (Y505H) present in all the Omicron sub-lineages is assumed to be highly deleterious owing to highly positive electrostatic surface potentials [58]. Our interaction and pathogenicity analysis revealed the His 505 interaction with Nb paratopes, which could be thought of as the possible outcome to reduce the affinity of RBD for ACE-2 receptors in the human body.

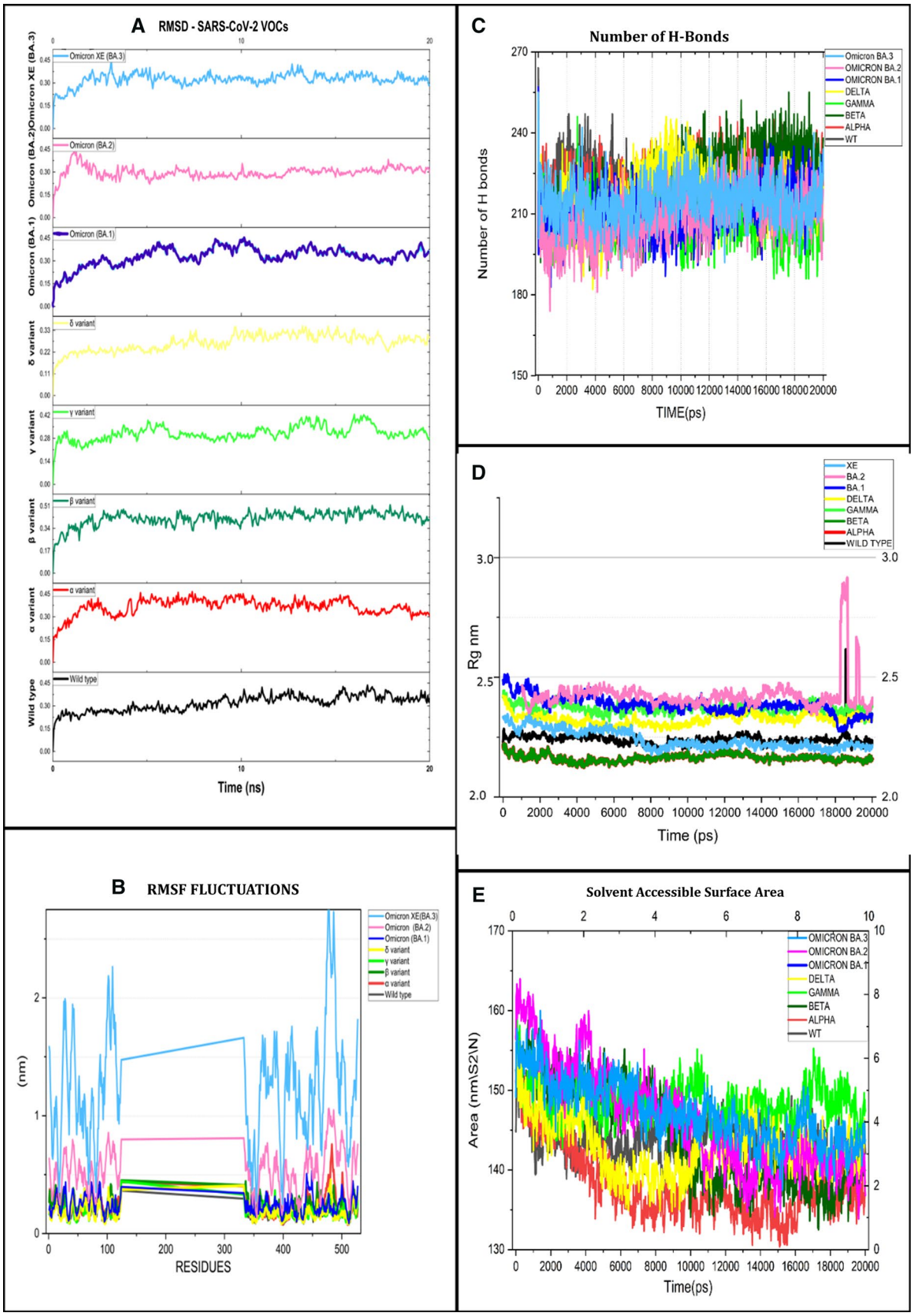
A
RMSD - SARS-CoV-2 VOCs
Omicron XE (BA.3)
Omicron (BA.2)
Omicron (BA.1)
δ variant
γ variant
β variant
α variant
Wild type
Time (ns)
B
RMSF FLUCTUATIONS
Omicron XE(BA.3)
Omicron (BA.2)
Omicron (BA.1)
δ variant
γ variant
β variant
α variant
Wild type
(nm)
RESIDUES
C
Number of H-Bonds
Omicron BA.3
OMICRON BA.2
OMICRON BA.1
DELTA
GAMMA
BETA
ALPHA
WT
Number of H bonds
TIME(ps)
D
XE
BA.2
BA.1
DELTA
GAMMA
BETA
ALPHA
WILD TYPE
Rg nm
Time (ps)
E
Solvent Accessible Surface Area
OMICRON BA.3
OMICRON BA.2
OMICRON BA.1
DELTA
GAMMA
BETA
ALPHA
WT
Area (nm\S2\N)
Time(ps)

◂**Fig. 7** Molecular Dynamics Simulation of Nb VHH W- RBD complex using WebGro web interface. **a** RMSD plots for all the VoCs RBD forming complex with Nb VHH W. **b** RMSF plot of Nb VHH W-RBD complexes. **c** Number of H-bonds present in the Nb VHH W –RBD complexes **d** Radius of Gyration of Nb VHH W-RBD complexes **e** SASA plot for the Nb VHH W –RBD complexes

Molecular dynamics simulation of Nb VHH W-VoC's RBD

Molecular dynamics simulations made feasible by the WebGRO server investigate macromolecular dynamics, such as protein–protein systems. MD simulations for 20 ns at 300 K temperature were undertaken on the Nb VHH W-RBDs complexes extracted from the CLUSPRO docking server for all of the chosen variants, and the data were compared [29]. To determine the stability and fluctuations of the aforementioned complexes, MD trajectories were analyzed in terms of RMSD (Root Mean Square Deviation), RMSF (Root Mean Square Fluctuation), RG (Radius of gyration), and SASA (Solvent Accessible Surface Area).

The RMSD of the protein backbone atoms is plotted against time in the graph to determine changes in structural conformation. Except for VHH W-Beta variant, RMSD graphs show that the other Nb-RBD complexes have the lowest variations in their RMSD below 0.5 nm and have attained a stable state during their dynamics' final stages. This depiction clearly shows the Nb's stability against the RBD of individual VoCs, while the complex underwent minor structural changes during the simulations (Fig. 7a).

RMSF is another significant criterion to consider that is used to investigate how the behavior of target protein amino acid residues changes when it binds to the RBD of the spike protein in the present case. The RMSF values for the Cα atoms were calculated and recorded against the residues. The Nb-RBD complexes RMSF pattern indicated similar fluctuations with a range below 0.5 nm, chiefly for Alpha, Gamma, Delta, and Omicron. The Nb VHH W in complex with the XE (BA.3) subvariant evidenced maximum fluctuation up to 2.5 nm during the dynamics of its interface residues in the RMSF plot. The fluctuations from 1 to 125 residues account for the Nanobody VHH W, whereas from 333 to 528 indicate the fluctuation for RBDs in the recorded complexes (Fig. 7b).

The concentration of H bonds at the proteins interface plays a critical role in governing the connection between two proteins together. Throughout the simulation, the number of H bonds at the Nb VHH W, and RBD-spike contact was displayed, revealing a wide range of H-bonds in the range from 180 to 200 in all the VoCs RBD complexes (Fig. 7c). In addition, the Radius of gyration was also determined to assess the compactness of the complex where a higher value indicates less compressed/compact packing and a lower value denotes tight, compact packing. During the simulation, the Nb VHH W/BA.2 RBD had fluctuations to higher values indicating the least compactness, whereas the Alpha and beta variant complex with Nb VHH W had the most compact packing with values below 2.5 nm throughout the simulation (Fig. 7d). Lastly, all the complexes were computed for a Solvent Accessible Surface Area (SASA) analysis for the interface residues of the complex for exploring the scope of receptor exposure to the surrounding solvent molecules where higher SASA values define for more exposed surface and vice versa. In a broad sense, the SASA plot revealed the highest score for Omicron BA.2 (above 160 nm^2), and other complexes were 145–160 nm^2 depicting the shift in the area in contact with the solvent. The variance in amino acid side chains and the pattern of amino acid composition at protein–protein interfaces culminated in a diverse number of interactions (Fig. 7e).

Affinity maturation by alanine scanning mutagenesis and assessment of binding affinity of mutant Nb

To advance the binding affinity of the Nb-RBD complex, affinity maturation was performed of the selected Nb VHH W through the in-silico alanine scanning mutagenesis experiment. All the contacting interface residues were preliminarily checked by mutating each to Ala, which was carried out using the DrugScore PPI server. The server did identify the critical hotspot ranking in terms of favorable $\Delta\Delta G$ score. Of the predicted mutations in the Nb VHH we selected, D29A, Y102A, and Y111A exhibited the most favorable $\Delta\Delta G$ scores (Supplementary Fig. 1). Additionally, it must be noted that D29A and Y111A belonged to CDR regions among the three selected mutants, while the Y102A was mapped at the framework region of Nb. To classify the mutant best suited for increasing the binding efficacy of Nb VHH W, single, double, and triple mutants were designed using the Wizard Mutagenesis tool of PyMol.

Further screening of the results in the CLUSPRO server for the three rounds of affinity maturation revealed that the single mutant Y111A exhibited a remarkable increase in affinity with better specificity to all the VoCs RBD as a target. Similar results were obtained in validation through the HDOCK server (Fig. 8, Table 3).

Physiochemical assessment and selection of antiviral peptide targeting ACE2 receptor

A large body of evidence suggests that small molecules such as peptides, neutralizing antibodies, nanobodies, or natural substances can efficiently mediate interaction with human ACE-2, making them a possible therapy option for COVID-19 patients. First, the 650 anti-viral peptides picked from the

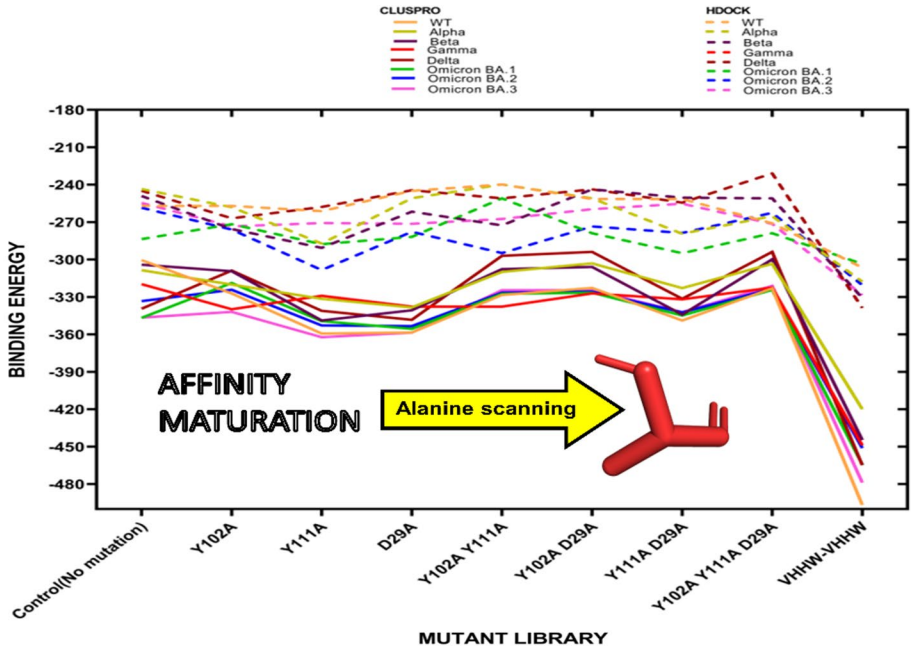

Fig. 8 Graphical account of the docking scores for the Alanine scanning mutagenesis generated mutant library for both CLUSPRO and HDOCK servers

Table 3 Binding energy of the Nb VHH W mutant library post Alanine scanning against VOCs RBD using CLUSPRO docking server and validated by HDOCK docking server

Round no	Mutants	WT		Alpha		Beta		Gamma	
		CLUSPRO	HDOCK	CLUSPRO	HDOCK	CLUSPRO	HDOCK	CLUSPRO	HDOCK
Round 0	Control(No mutation)	− 300.5	− 256.99	− 308.5	− 243.55	− 304.1	− 249.04	− 319.7	− 249.04
Round 1	Y102A	− 327.2	− 256.99	− 320.1	− 258.07	− 309.4	− 275.6	− 339.8	− 275.6
	Y111A	− 359.3	− 261.2	− 331.5	− 287.2	− 348.9	− 290.6	− 329.1	− 290.6
	D29A	− 358.5	− 244.93	− 338.4	− 250.82	− 340.7	− 261.6	− 337.8	− 261.6
Round 2	Y102A Y111A	− 328.4	− 239.81	− 309.9	− 239.81	− 307.7	− 272.62	− 337.7	− 272.62
	Y102A D29A	− 322.8	− 251.5	− 303.1	− 250.9	− 305.9	− 243.69	− 327.2	− 243.69
	Y111A D29A	− 348.8	− 251.5	− 322.9	− 279.28	− 344.1	− 250.45	− 331.9	− 250.45
Round 3	Y102A Y111A D29A	− 323.1	− 270.92	− 303.4	− 265.21	− 299.8	− 250.9	− 322.5	− 250.9
DIMER	VHHW-VHHW	− 496.7	− 306.48	− 420	− 317.77	− 444.7	− 330.82	− 449	− 330.82
Round no	Mutants	Delta		Omicron (BA.1)		Omicron(BA.2)		Omicron(BA.3)	
		CLUSPRO	HDOCK	CLUSPRO	HDOCK	CLUSPRO	HDOCK	CLUSPRO	HDOCK
Round 0	Control(No mutation)	− 339.4	− 244.89	− 346.8	− 283.62	− 333.4	− 258.49	− 346.5	− 254.61
Round 1	Y102A	− 308.9	− 267	− 318.8	− 271.64	− 324.2	− 275.98	− 341.9	− 273.43
	Y111A	− 341.1	− 257.8	− 349.4	− 287.69	− 352.8	− 308.43	− 362.2	− 270.8
	D29A	− 348.3	− 244.42	− 355.5	− 281.79	− 353.3	− 277.74	− 358.6	− 271.34
Round 2	Y102A Y111A	− 297	− 250.98	− 327.5	− 250.98	− 326.5	− 294.8	− 324.6	− 267.47
	Y102A D29A	− 293.9	− 243.67	− 326.5	− 278.93	− 325.7	− 273.49	− 324.6	− 259.67
	Y111A D29A	− 331.5	− 254.44	− 344.9	− 294.91	− 342.4	− 278.72	− 342.1	− 255.26
Round 3	Y102A Y111A D29A	− 293.9	− 230.9	− 324.3	− 278.93	− 323.4	− 262.53	− 321.1	− 271.31
DIMER	VHHW-VHHW	− 464.9	− 338.84	− 464.2	− 303.54	− 451.2	− 320.46	− 478.8	− 328.41

AVPdb database were tested to determine that they specifically prevented viral entry. Several factors were considered while sorting a desirable AVP, including length, antigenicity, allergenicity, toxicity, solubility in water, and stability. The first parameter we used was the length; we chose 15-amino-acid peptides. Following that, we ensured that the peptides we chose were non-allergenic, non-toxic, and antigenic. In the VaxiJen 2.0 server, the cutoff score for antigenicity was

set to > 0.5. Ultimately, the peptide must be water-soluble and exceedingly stable, considering all of the preceding factors. In the end, we were left with five peptides whose FASTA sequences were preserved for docking against the hACE-2 receptor.

Prior to AVP docking and assemblage to the Nb, a dithiocyclopeptide linker was picked from the documented studies for linking the AVP to the Nb. The dithiocyclopeptide linker (LEAGCKNFFPRSFTSCGSLE) is a disulfide blood cleavable linker that could leave as soon as the Nb construct encounters the blood proteases and enzymes. Hence, the protease cleavage site was first detected with the help of PEPTIDE CUTTER and PROSPER web servers. The results revealed the cleavage site in LEAGCKNFFPRS*FTSCGSLE, between S(Ser) and F (Phe), which could be cleaved by the Metalloprotease and Thrombin serine protease. The protease mediates cleavage in its C-terminal direction towards the right side of the marked amino acid. As a result, the FTSCGSLE component of the linker is anticipated to remain linked to the AVP once the proteases have cleaved it. Looking at the whole picture, the peptide model was created, and docking was performed using HDOCK. The HDOCK protein–protein docking server offers a rich media to accept PDB and FASTA input files and perform template-based modeling, which allowed us to feed the partly-linker-added-AVP to dock with the ACE-2 PDB structure (7WBL)[59].

This was implemented for each of the five AVP contestants, and the model with the lowest binding energy was chosen for future investigation. S19, Q24, K31, H34, E35, E37, D38, Y41, Y83, and K353 are ten primary amino acid residues interacting with the spike RBD hotspot. The docking was done site-specific, with the AVP targeting the ACE-2 hotspot residues. As a result, the critical interacting ACE-2 interface residues were also accepted as selection criteria in addition to the binding energy. We chose the AVP0725 peptide, which was used to block ACE-2 and SARS-CoV-2 RBD interactions and was further integrated with the Nb utilizing a blood cleavable linker (Table 4).

Designing and validation of biparatopic nanobody peptide construct

We introduced a second mutant Nb VHH W with the single mutant Nb VHH W intending to further boost the Nb's potency against all the VoCs RBD. The homodimer was generated by joining the entities with $(GGGGS)_3$ flexible linkers. Ultimately, the whole construct was achieved by arranging the FASTA sequence of each component in the series from N' to C' as mutant Nb VHH W-$(GGGGS)_3$ flexible linker- mutant Nb VHH W-Dithiocyclopeptide blood cleavable linker-Antiviral peptide AVP075 and feeding it to the I-Tasser modeling tool. The model assembly was created,

Table 4 List of top 5 Antiviral peptides taken from AVPdb and their docking assessment with hACE-2 receptor

S. no.	AVPred ID	Sequences (15 amino acid)	Physiological target	Allergenicity	Antigenicity	Solubility	Half-life (stability)	FTSCGSLE + AVP	Binding energy	Interacting ACE-2 hotspots
1	AVP0771	EQSRKPPNPT-PPPPG	Viral entry	Non allergen	Antigen	Good water solubility	6.347	FTSCG-SLEEQSRKPP-NPTPPPPG	-121.48	K31, E35, Y83
2	AVP0691	AAPTGDPKPK-KNKKP	Viral entry	Non allergen	Antigen	Good water solubility	6.347	FTSCGSLEAAPTG-DPKPKKNKKP	-98	H34, E37, K353
3	AVP0725	DMELKPA-NAATRTSR	Viral entry	Non allergen	Antigen	Good water solubility	2.191	FTSCGSLED-MELKPA-NAATRTSR	-132.38	Q24, K31, H34, E35, D38, Y83, K353
4	AVP0799	TRDAIEPCT-VGHRRY	Viral entry	Non allergen	Antigen	Good water solubility	0.791	FTSCGS-LETRDAIEPCT-VGHRRY	-138.83	Q24, K31, E35, D38, Y83
5	AVP0759	RVDLGDCIGKD-ARDA	Viral entry	Non allergen	Antigen	Good water solubility	0.646	FTSCGSLERVDLG-DCIGKDARDA	-87.31	S19, Q24, K31, H34, E35, E37, D38, Y83, K353

so neither the linker nor the AVP interfered with the CDR region of the selected Nb. The selection of the 3D model was based on the benchmarked scoring system, such as the confidence score. It estimated the TM score, which was measured as − 2.32 and 0.440 ± 14, respectively, to evaluate the I-TASSER model's quality. We obtained a 3D biparatopic Nb-peptide conjugate in.pdb format. Next, the final construct with Nb dimer was docked against the RBDs to validate the increase in its binding efficiency. CLUSPRO and HDOCK servers both revealed a substantial rise in their scores, indicating a significant improvement in binding energy over many folds (Fig. 8, Table 3). The quality of the model was validated by evaluating various structural aspects determining the quality of the model. The ProSA web server depicts that the more significant portion of the energy plot lies in the highly negative region, suggesting negligible problematic or error regions in the structural model. In addition, the Z score graph determined by the X-ray and NMR spectroscopy gives

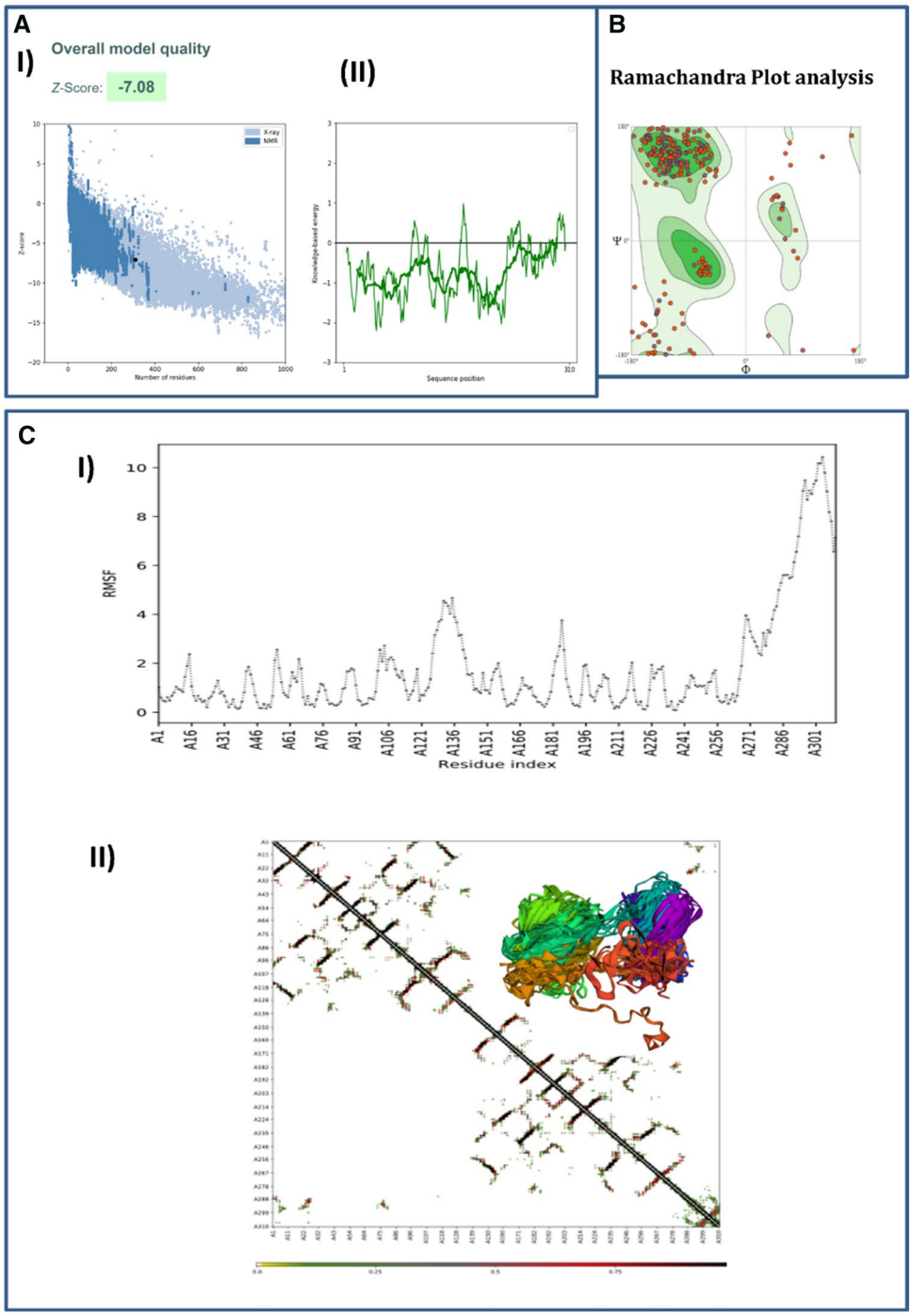

Fig. 9 3D Model validation for the biparatopic NPC **a** ProSA web generated I) Z plot showing -7.08 score and II) Energy plot of the predicted structure for all residues. **b** Ramachandran plot showcasing the presence of amino acid residues in the favoured, allowed, and outlier zones. **c** (I) CABS-Flex derived Root Mean Square Fluctuation (RMSF) during simulation. (;II) Contact map representing the frequency of contacts of the trajectory profiles of the biparatopic NPC

the location of the Z score to be − 7.08, which lies in the range of native conformation and represents a good quality model (Fig. 9a (I) (II)). The structure assessment was done using the SWISS-MODEL tool, where the RC plot analysis showed 82.47% favored residues (Fig. 9b). Lastly, the antiviral Nb flexibility is the crucial aspect of its performance; hence, to predict the structural protein flexibility, simulations in CABSflex were run at 1.4 °C temperature with 50 cycles. Our biparatopic conjugate showed an elevated level of fluctuations at the residue index 286, 296, and 304, which was documented to be 5.606 Å, 9.48 Å, and 10.43 Å in that order. In addition, the server also provided the contact map where each dot represents the frequency of contacting pairs of the trajectory final complex. Based on the frequency of occurrence, the darker color code signifies high probability (1), and the lighter color represents low probability (0) of residue contacts in a binary fashion (Fig. 9c (I) (II)).

PEGylation, physiochemical, and toxicological validation of final construct

The biparatopic Nb-peptide-conjugate was compared to the existing Nb VHH W taken as a control for physiochemical and toxicological traits, which could be used in in vitro investigations to eliminate any off-target or side effects. Impressively, the built biparatopic Nb outperformed the conventional nonmutated Nb on all calculated metrics such as molecular weight, thermostability, pI, solubility, and half-life of the construct in blood, toxicity, antigenicity, and allergenicity. It's worth noting that the proposed biparatopic NPC has a longer half-life of 1498.01 s, a higher pI of 5.63, and a thermostability of 67.9 °C, all of which are considerable improvements over regular Nb just except for the reduced solubility. The mutant Nb VHH biparatope has been reported. The mutant Nb VHH W biparatope was shown to be antigenic, non-allergenic, and non-toxic and have advanced immunogenic qualities (Table 5).

Lastly, PEGylation of the whole construct gave the insight to amplify the existing biparatopic Nb peptide conjugate to many folds, thus limiting its rapid renal clearance and other stability constraints. A 20 kDa linear maleimide-terminated PEG (MAL-$(PEG)_n$-OMe) linker is commonly used as a PEGylating agent to increase the efficacy and specificity of antibody-like format. We specifically attached the PEG linker to the Cysteine 22 at the second Nb VHH W on its N terminal end to overall stabilize the entity. Visualization of the construct after all the modifications was done using Schrodinger Maestro software [60] (Fig. 10a).

In silico cloning in yeast display expression vector

The study's ultimate purpose was to clone the designed biparatopic Nb peptide construct (NPC) into a eukaryotic expression vector, i.e., yeast display vector pPICZαA, to amplify the yield and express it seamlessly by anyone [61]. The output obtained from the NEBcutter tool shows the absence of any commercially available restriction sites. While the VectorBuilder tool denoted the CAI value for the biparatopic NPC to be 0.91, which lies within the ideal range of 0.8–1.0, suggesting a good expression. At the same time, the sequence's GC content was calculated as 59.59%, which also falls under the ideal range. The optimized codon sequence was then reversed, and Acc65I and XbaI restriction site's introduction to the N- and C-terminal of the optimized sequence complemented the translation direction of the pPICZαA-Pichia pastoris expression vector. Finally, the SnapGene tool and restriction cloning performed into the pPICZαA expression system resulted in a length of

Table 5 Comparing the therapeutic efficacy of conventional Nb VHH W vs prospective Biparatopic Nb VHH W-peptide-conjugate

S. no.	Parameters (Physiochemistry/Toxicity)	*In-silico* Server	Nb VHH W	Biparatopic Nb VHH W-peptide-conjugate
1	Molecular Wt	ExPasy Protparam	13,379.69 Da	33,097.25 Da
2	Half-life of peptide in blood	pLifePred	1485.91 s	1498.01 s
3	pI	ExPasy Protparam	5.57	5.63
4	Solubility	ProteinSol	0.525	0.453
5	Thermostability	SCooP	63.2 °C	67.9 °C
6	Toxicity	ToxinPred	Non-Toxic	Non-Toxic
7	Allergenicity	Algpred	NON-ALLERGEN (-0.4122545)	NON-ALLERGEN (-0.46132856)
8	Antigenicity	VaxiJen 2	Antigen (0.4541)	Antigen (0.5102)

5510 base pairs, where our desired GOI (biparatopicNPC)

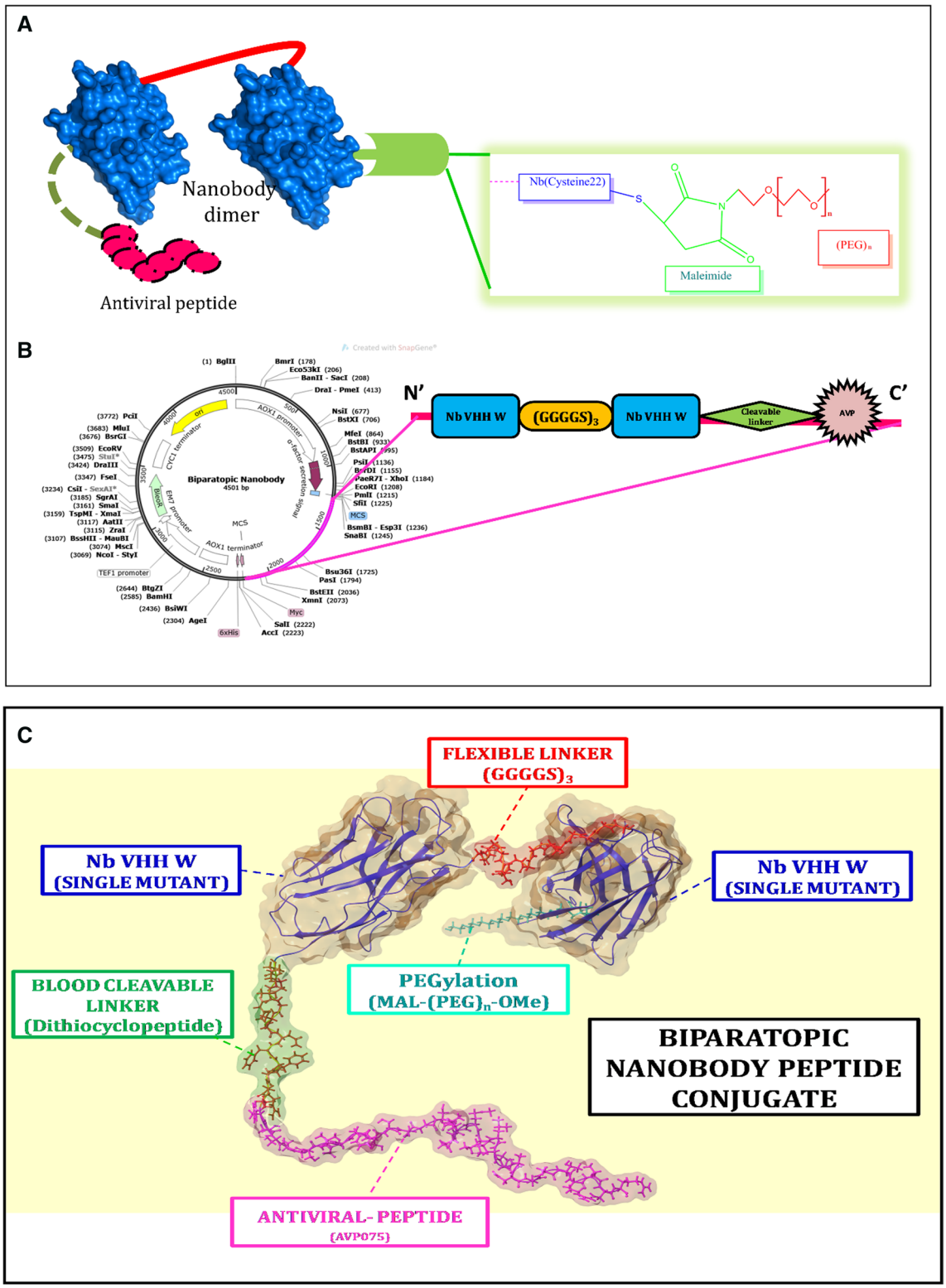

Fig. 10 **a** PEGylation of the Biparatopic Nanobody conjugate with 20 kDa linear maleimide-terminated PEG (MAL-$(PEG)_n$-OMe) linker. **b** Schematic design of *in-silico* cloning vector map showing the insert of biparatopic NPC with specific optimized codons with gene of interest-biparatopic NPC (magenta) into the pPICZαA-Pichia pastoris expression vector (www.SnapGene.com). **c** The final design of the biparatopic nanobody-peptide-conjugate prepared using Schrodinger Maestro software

constitutes a 933-base pair (Fig. 10b). Visualization of the construct after all the modifications was done using Schrodinger Maestro software whose output is displayed [60] (Fig. 10c).

Discussion

The episode of the COVID-19 crisis has introduced the dynamic nature of the causal pathogen, the SARS-CoV-2 virus. The lethal virus's ability to alter its genetic makeup at such a tremendous rate, as well as its potential to trigger epidemics in a multitude of locations, has prompted scientists to seek a substitute cure. The focus is on a subset of mutants that can undergo mutations, exacerbate the disease status, and elude the established treatment procedure, ensuing in a spike in death toll figures. Looking at the global risk quotient, WHO has addressed these mutants as variants of concern; by now, Alpha, Beta, Gamma, Delta, Omicron, and their sub-lineages have been acknowledged as the established VoCs originating as outbreak epicenters across several continents [2, 62, 63].

The earliest mutations were able to be drifted by healthcare experts, but the more recent mutants have rendered the commonly used monoclonal antibodies and convalescence sera treatment useless after vaccines. When sources claim that the Delta variant is more pathogenic or the substantially altered Omicron strain is more transmissible, skepticism about the vaccines' efficacy intensifies [64–66]. Inflammatory reactions to vaccination have also been recorded in a population subgroup. While many of the studies have already adapted to work with well-documented neutralizing antibodies, repurposed drugs, antiviral, and peptidomimetics approaches, the question of whether these approaches will be enough to mitigate the upcoming threat of a more pathogenic and transmissible pan coronavirus remains unanswered [67].

Passive immunotherapy, such as monoclonal antibodies (mAbs), is a promising strategy to combat circulating variants. Still, it has hit a roadblock since the evolving virus has begun to accumulate escape mutations. To join these gaps, we tried to haul antibodies-like nanobodies to assess their efficacy as a substitute. Thermal stability, ease of synthesis, stability, and the capacity to be easily conjugated with tiny druggable molecules, as well as the ability to tailor them into multimers, qualify them as possible therapeutic options [68–70].

While much of the research has concentrated on the virus's spike glycoprotein, which contains the RBD, it is believed to be a critical viral component that interacts with the hACE-2 receptor to penetrate the host cell. At the same time, by undergoing mutation, this RBD can rearrange its architecture to increase its affinity for the hACE2 receptor, allowing it to bypass the host immune response.

The perspective of the present study was to utilize the dynamicity of computational immunoinformatics approaches to remodel a highly effective nanobody centered on pharmacokinetic properties and binding efficiencies computed against VoC RBDs [71]. Physiochemical characterization allows for the early preclinical screening of the best Nb, which can drastically minimize the time and expense required to de-risk the conjugate drug development process [72]. The biophysical evaluation of 45 sorted Nb indicated a sufficient cationic pI (mostly above 6) and high-temperature resistance (> 60 **°C**), simplifying manufacture, storage, and shelf life extension, all of which are desirable properties in a therapeutic candidate [73]. Next, we used a computational pipeline in our study to examine the Nbs binding affinity via antibody-antigen docking studies against the spike RBD for a panel of SARS-CoV-2 VoCs and a brief comprehension of its dynamics. The screening procedure facilitated qualifying the Nb VHH W as our protagonist for downstream analysis based on its picomolar binding affinity against all the VoCs RBDs since immunoglobulins with high affinity is typically in the picomolar range [74]. The majority of the conserved epitopes from practically all of the presented variants could bind to the residue found in the Nb VHH W CDR loops, which are expanded and exposed in the case of Nbs, providing a similar or better binding affinity than mAbs [75]. We reported a striking increment in the binding energy, binding affinity, and Kd following affinity maturation of the Nb VHH W as a single mutant Y111A against all the reported VoCs RBD [76]. Thermal stability, ease of synthesis, stability, and the capacity to be easily conjugated with tiny druggable molecules, as well as the ability to tailor them into multimers, qualify them as possible anti-SARS-CoV-2 therapeutic options. Consequently, it was asserted that introducing a single mutant Nb VHH W entity to make an Nb homodimer raised the binding strength by several magnitudes. One of the homodimer's monomers, Nb, was computationally conjugated to a relatively small antiviral peptide that might block the ACE-2 receptor's entry. Later we conjugated this with an AVP0725 anti-viral peptide with the help of a disulphide blood protease cleavable linker to increase the half-life, stability, and effectiveness of the conjugate. This could successfully block the hotspot ACE-2 residues, overall ensuring the obstruction of RBD attachment to ACE-2 making it multispecific in nature. The dithiocyclopeptide blood linker fastens the antiviral peptide with Nb and cleaves as soon as it is released into the blood

circulation. This attachment breaks after encountering the proteases in the blood that finally separates the two entities (Nb dimer & AVP) to their respective targets.

Despite its many advantages, the nanobody is limited in its ability to excrete quickly due to its small size. As a result, the framework was PEGylated with a 20 kDa MAL-(PEG) n-OMe linker to enhance the overall drug's size, restricting renal clearance and prolonging the biparatopic construct's lifetime. In addition, in silico cloning was used in this study to support future neutralizing of NPC's expression using a yeast display *P. pastoris* expression system. The scope of the designed biparatopic NPC conjugate in the present work resulted in a therapeutic construct with marked supremacy over the conventional Nb VHH W in terms of pharmacokinetic backgrounds.

As a result, experimental studies on NPC are expected to show impressive outcomes in blocking viral entry by potentially reducing the risk of SARS-CoV-2 infection progression, promoting the culture of passive immunotherapy further. Undoubtedly, our research provides a great illustration of utilizing the velocity of computational biology to produce a highly viable class of nanoscale biologics or nanobodies to push the pharmacological status of COVID-19 beyond what's attainable. It might easily be integrated alongside current practices to reach the goal of a pan coronavirus therapy while reducing the overall burden on the pharmaceutical business in a resource and budget-friendly manner.

Conclusion

The present study gives a good blueprint for systematically mapping neutralizing epitopes, understanding the structural basis, and design a candidate Nb construct with multiple specificities which could uniquely target the spike of the SARS-CoV-2 VoCs to inhibit the virus and their variants. The rationale of this study could aid in designing of a pan-coronavirus therapies and vaccines. While further characterization and investigation are desired, this study drives a notion of presenting a combinatorial approach in COVID-19 treatment, which consists of an Nb effective against all the RBDs of VoCs with AVP, which is effective against the hACE-2 receptor. The fate of this small biparatopic NPC is optimistic about the potential outcome of developing cost-effective, stable, and safe nanobody-based therapeutics for inhaled use or intravenous routes in formal healthcare settings.

Supplementary Information The online version contains supplementary material available at https://doi.org/10.1007/s11030-022-10570-x.

Acknowledgements MP and EK is thankful to Central University for lab facilities. SS is thankful to Central University of Rajasthan for fellowship. VKP is thankful to the Central University of Rajasthan for providing lab facility.

Author contribution MP: Conceptualization, Data curation, Software analysis and Validation, Writing original draft. EK: Conceptualization, Data curation, Software analysis and Validation, Writing original draft. SS: Conceptualization, Data curation, Software analysis and Validation, Writing original draft. KK: Visualization, Writing—review & editing. VKP**:** Conceptualization, Supervision, Writing original draft and finalizing draft.

Funding No funding is available for the research.

Declarations

Conflict of interest Authors have declared no competing interest.

References

1. Shu Y, McCauley J (2017) GISAID: Global initiative on sharing all influenza data–from vision to reality. Eurosurveillance 22(13):30494. https://doi.org/10.2807/1560-7917.ES.2017.22.13.30494
2. ORGANIZATION, W.H. (2022) Tracking SARS-CoV-2 variants, WHO, Editor. WHO.
3. Chames P, Van Regenmortel M, Weiss E, Baty D (2009) Therapeutic antibodies: successes, limitations and hopes for the future. Br J Pharmacol 157(2):220–233. https://doi.org/10.1111/j.1476-5381.2009.00190.x
4. Sheridan C (2017) Ablynx's nanobody fragments go places antibodies cannot. Nat Biotechnol 35(12):1115–1118. https://doi.org/10.1038/nbt1217-1115
5. Sun D, Sang Z, Kim YJ, Xiang Y, Cohen T, Belford AK, Huet A, Conway JF, Sun J, Taylor DJ, Schneidman-Duhovny D (2021) Potent neutralizing nanobodies resist convergent circulating variants of SARS-CoV-2 by targeting diverse and conserved epitopes. Nat Commun 12(1):1–14
6. Hanke L, Vidakovics Perez L, Sheward DJ, Das H, Schulte T, Moliner-Morro A, Corcoran M, Achour A, Karlsson Hedestam GB, Hällberg BM, Murrell B (2020) An alpaca nanobody neutralizes SARS-CoV-2 by blocking receptor interaction. Nat Commun 11(1):1–9. https://doi.org/10.1038/s41467-020-18174-5
7. Xu J, Xu K, Jung S, Conte A, Lieberman J, Muecksch F, Lorenzi JCC, Park S, Schmidt F, Wang Z, Huang Y (2021) Nanobodies from camelid mice and llamas neutralize SARS-CoV-2 variants. Nature 595(7866):278–282. https://doi.org/10.1038/s41586-021-03676-z
8. Benson DA, Karsch-Mizrachi I, Lipman DJ, Ostell J, Wheeler DL (2012) GenBank. Nucleic Acids Res 41(D1):D36–D42. https://doi.org/10.1093/nar/gkw1070
9. Güttler T, Aksu M, Dickmanns A, Stegmann KM, Gregor K, Rees R, Taxer W, Rymarenko O, Schünemann J, Dienemann C, Gunkel P (2021) Neutralization of SARS-CoV-2 by highly potent, hyperthermostable, and mutation-tolerant nanobodies. EMBO J 40(19):e107985. https://doi.org/10.15252/embj.2021107985
10. Sievers F, Higgins DG (2014) Clustal omega. Curr Protoc Bioinform 48(1):3131–31316. https://doi.org/10.1002/0471250953.bi0313s48
11. Gouet P, Courcelle E, Stuart DI, Metoz F (1999) ESPript: analysis of multiple sequence alignments in PostScript. Bioinformatics (Oxford, England) 15(4):305–308. https://doi.org/10.1093/bioinformatics/15.4.305

12. Schwede T, Kopp J, Guex N, Peitsch MC (2003) SWISS-MODEL: an automated protein homology-modeling server. Nucleic Acids Res 31(13):3381–3385. https://doi.org/10.1093/nar/gkg520
13. Giardine B, Riemer C, Hardison RC, Burhans R, Elnitski L, Shah P, Zhang Y, Blankenberg D, Albert I, Taylor J, Miller W (2005) Galaxy: a platform for interactive large-scale genome analysis. Genome Res 15(10):1451–1455. https://doi.org/10.1101/gr.4086505
14. Raybould MI, Kovaltsuk A, Marks C, Deane CM (2021) CoV-AbDab: the coronavirus antibody database. Bioinformatics 37(5):734–735. https://doi.org/10.1093/bioinformatics/btaa739
15. Berman H, Henrick K, Nakamura H, Markley JL (2007) The worldwide Protein Data Bank (wwPDB): ensuring a single, uniform archive of PDB data. Nucleic Acids Res 35(1):D301–D303. https://doi.org/10.1093/nar/gkl971
16. Delano WL (2002) Pymol: An open-source molecular graphics tool. CCP4 Newsl. Protein Crystallogr. 40(1):82–92
17. Ko J, Park H, Heo L, Seok C (2012) GalaxyWEB server for protein structure prediction and refinement. Nucleic Acids Res 40(W1):W294–W297. https://doi.org/10.1093/nar/gks493
18. Hebditch M, Carballo-Amador MA, Charonis S, Curtis R, Warwicker J (2017) Protein–Sol: a web tool for predicting protein solubility from sequence. Bioinformatics 33(19):3098–3100. https://doi.org/10.1093/bioinformatics/btx345
19. Sharma A, Singla D, Rashid M, Raghava GPS (2014) Designing of peptides with desired half-life in intestine-like environment. BMC Bioinform 15(1):1–8. https://doi.org/10.1186/1471-2105-15-282
20. Pucci F, Kwasigroch JM, Rooman M (2017) SCooP: an accurate and fast predictor of protein stability curves as a function of temperature. Bioinformatics 33(21):3415–3422. https://doi.org/10.1093/bioinformatics/btx417
21. Glaser F, Pupko T, Paz I, Bell RE, Bechor-Shental D, Martz E, Ben-Tal N (2003) ConSurf: identification of functional regions in proteins by surface-mapping of phylogenetic information. Bioinformatics 19(1):163–164. https://doi.org/10.1093/bioinformatics/19.1.163
22. Bendl J, Stourac J, Salanda O, Pavelka A, Wieben ED, Zendulka J, Brezovsky J, Damborsky J (2014) PredictSNP: robust and accurate consensus classifier for prediction of disease-related mutations. PLoS Comput Biol 10(1):e1003440. https://doi.org/10.1371/journal.pcbi.1003440
23. Kozakov D, Hall DR, Xia B, Porter KA, Padhorny D, Yueh C, Beglov D, Vajda S (2017) The ClusPro web server for protein–protein docking. Nat Protoc 12(2):255–278. https://doi.org/10.1038/nprot.2016.169
24. Abbasi WA, Hassan FU, Yaseen A, Minhas FUAA (2017) ISLAND: In-silico prediction of proteins binding affinity using sequence descriptors. arXiv preprint arXiv:1711.10540.
25. Moxon R, Reche PA, Rappuoli RJFII (2019) Reverse vaccinology. Curr Opin Microbiol 3(5):445–450. https://doi.org/10.3389/fimmu.2019.02776
26. Kaas Q, Lefranc M-P (2007) IMGT Colliers de Perles: standardized sequence-structure representations of the IgSF and MhcSF superfamily domains. Curr Bioinform 2(1):21–30. https://doi.org/10.1093/bfgp/elm032
27. Wallace AC, Laskowski RA, Thornton JM (1995) LIGPLOT: a program to generate schematic diagrams of protein-ligand interactions. Protein Eng Des Sel 8(2):127–134. https://doi.org/10.1093/protein/8.2.127
28. Singh S, Kumar K, Panda M, Srivastava A, Mishra A, Prajapati VK (2022) High-throughput virtual screening of small-molecule inhibitors targeting immune cell checkpoints to discover new immunotherapeutics for human diseases. Mol Divers. https://doi.org/10.1007/s11030-022-10452-2
29. Bekker H, Berendsen HJC, Dijkstra EJ, Achterop S, Vondrumen R, Vanderspoel D, Sijbers A, Keegstra H, Renardus MKR (1993) Gromacs-a parallel computer for molecular-dynamics simulations. In 4th International Conference on Computational Physics (PC 92). World Scientific Publishing, pp 252–256
30. Singh S, Prajapati VK (2022) Exploring actinomycetes natural products to identify potential multi-target inhibitors against Leishmania donovani. 3 Biotech 12(9):235. https://doi.org/10.1007/s13205-022-03304-1
31. Krüger DM, Gohlke H (2010) DrugScorePPI webserver: fast and accurate in silico alanine scanning for scoring protein–protein interactions. Nucleic Acids Res 38(2):W480–W486. https://doi.org/10.1093/nar/gkq471
32. Yan Y, Zhang D, Zhou P, Li B, Huang SY (2017) HDOCK: a web server for protein–protein and protein–DNA/RNA docking based on a hybrid strategy. Nucleic Acids Res 45(W1):W365–W373. https://doi.org/10.1093/nar/gkx407
33. Qureshi A, Thakur N, Tandon H, Kumar M (2014) AVPdb: a database of experimentally validated antiviral peptides targeting medically important viruses. Nucleic Acids Res 42(D1):D1147–D1153. https://doi.org/10.1093/nar/gkt1191
34. Saha S, Raghava GPS (2006) AlgPred: prediction of allergenic proteins and mapping of IgE epitopes. Nucleic Acids Res 34(2):W202–W209. https://doi.org/10.1093/nar/gkl343
35. Gupta S, Kapoor P, Chaudhary K, Gautam A, Kumar R (2013) In silico approach for predicting toxicity of peptides and proteins. PLoS ONE 8(9):e73957. https://doi.org/10.1371/journal.pone.0073957
36. Doytchinova IA, Flower DR (2007) VaxiJen: a server for prediction of protective antigens, tumour antigens and subunit vaccines. BMC Bioinform 8(1):1–7. https://doi.org/10.1186/1471-2105-8-4
37. Lear S, Cobb SL (2016) Pep-Calc com: a set of web utilities for the calculation of peptide and peptoid properties and automatic mass spectral peak assignment. J Comput-aided Mol Des 30(3):271–277. https://doi.org/10.1007/s10822-016-9902-7
38. Xiang Y, Nambulli S, Xiao Z, Liu H, Sang Z, Duprex WP, Schneidman-Duhovny D, Zhang C, Shi Y (2020) Versatile and multivalent nanobodies efficiently neutralize SARS-CoV-2. Science 370(6523):1479–1484. https://doi.org/10.1126/science.abe4747
39. Chen X, Bai Y, Zaro JL, Shen WC (2010) Design of an in vivo cleavable disulfide linker in recombinant fusion proteins. Biotechniques 49(1):513–518. https://doi.org/10.2144/000113450
40. Song J, Tan H, Perry AJ, Akutsu T, Webb GI, Whisstock JC, Pike RN (2012) PROSPER: an integrated feature-based tool for predicting protease substrate cleavage sites. PLoS ONE 7(11):e50300. https://doi.org/10.1371/journal.pone.0050300
41. Gasteiger E, Hoogland C, Gattiker A, Wilkins MR, Appel RD, Bairoch A (2005) Protein identification and analysis tools on the ExPASy server. The proteomics protocols handbook, pp571–607. doi: https://doi.org/10.1385/1-59259-584-7:531.
42. Zhang Y (2008) I-TASSER server for protein 3D structure prediction. BMC Bioinform 9(1):1–8. https://doi.org/10.1186/1471-2105-9-40
43. Kuriata A, Gierut AM, Oleniecki T, Ciemny MP, Kolinski A, Kurcinski M, Kmiecik S (2018) CABS-flex 2.0: a web server for fast simulations of flexibility of protein structures. Nucleic Acids Res 46(W1):W338–W343. https://doi.org/10.1093/nar/gky356
44. Kiefer F, Arnold K, Künzli M, Bordoli L, Schwede T (2009) The SWISS-MODEL Repository and associated resources. Nucleic Acids Res 37(1):D387–D392. https://doi.org/10.1093/nar/gkn750

45. Wiederstein M, Sippl MJ (2007) ProSA-web: interactive web service for the recognition of errors in three-dimensional structures of proteins. Nucleic Acids Res 35(2):W407–W410. https://doi.org/10.1093/nar/gkm290
46. Gasteiger E, Gattiker A, Hoogland C, Ivanyi I, Appel RD, Bairoch A (2003) ExPASy: the proteomics server for in-depth protein knowledge and analysis. Nucleic Acids Res 31(13):3784–3788. https://doi.org/10.1093/nar/gkg563
47. Francis GE, Fisher D, Delgado C, Malik F, Gardiner A, Neale D (1998) PEGylation of cytokines and other therapeutic proteins and peptides: the importance of biological optimisation of coupling techniques. Int J Hematol 68(1):1–18. https://doi.org/10.1016/s0925-5710(98)00039-5
48. Vincze T, Posfai J, Roberts RJ (2003) NEBcutter: a program to cleave DNA with restriction enzymes. Nucleic Acids Res 31(13):3688–3691. https://doi.org/10.1093/nar/gkg526
49. Xi X, Sun W, Li H, Fan Q, Zhang X, Sun F (2021) A comparative study and evaluation of anti-EGFR nanobodies expressed in Pichia pastoris and *Escherichia coli* as antitumor moieties. Protein Expr Purif 184:105888. https://doi.org/10.1016/j.pep.2021.105888
50. Li T, Cai H, Yao H, Zhou B, Zhang N, van Vlissingen MF, Kuiken T, Han W, GeurtsvanKessel CH, Gong Y, Zhao Y (2021) A synthetic nanobody targeting RBD protects hamsters from SARS-CoV-2 infection. Nat Commun 12(1):1–13. https://doi.org/10.1038/s41467-021-24905-z
51. Yang Z, Wang Y, Jin Y, Zhu Y, Wu Y, Li C, Kong Y, Song W, Tian X, Zhan W, Huang A (2021) A non-ACE2 competing human single-domain antibody confers broad neutralization against SARS-CoV-2 and circulating variants. Signal Transduct Target Ther 6(1):1–8. https://doi.org/10.1038/s41392-021-00810-1
52. Koenig PA, Das H, Liu H, Kümmerer BM, Gohr FN, Jenster LM, Schiffelers LD, Tesfamariam YM, Uchima M, Wuerth JD, Gatterdam K (2021) Structure-guided multivalent nanobodies block SARS-CoV-2 infection and suppress mutational escape. Science 371(6530):eaber6230. https://doi.org/10.1126/science.abe6230
53. Pymm P, Adair A, Chan LJ, Cooney JP, Mordant FL, Allison CC, Lopez E, Haycroft ER, O'Neill MT, Tan LL, Dietrich MH (2021) Nanobody cocktails potently neutralize SARS-CoV-2 D614G N501Y variant and protect mice. Proc Natl Acad Sci 118(19):e2101918118. https://doi.org/10.1073/pnas.2101918118
54. Custódio TF, Das H, Sheward DJ, Hanke L, Pazicky S, Pieprzyk J, Sorgenfrei M, Schroer MA, Gruzinov AY, Jeffries CM, Graewert MA (2020) Selection, biophysical and structural analysis of synthetic nanobodies that effectively neutralize SARS-CoV-2. Nat Commun 11(1):1–11. https://doi.org/10.1038/s41467-020-19204-y
55. Obr M, Ricana CL, Nikulin N, Feathers JPR, Klanschnig M, Thader A, Johnson MC, Vogt VM, Schur FK, Dick RA (2021) Structure of the mature Rous sarcoma virus lattice reveals a role for IP6 in the formation of the capsid hexamer. Nat Commun 12(1):1–12. https://doi.org/10.1038/s41467-021-23506-0
56. Koenig PA, Das H, Liu H, Kümmerer BM, Gohr FN, Jenster LM, Schiffelers LD, Tesfamariam YM, Uchima M, Wuerth JD, Gatterdam K (2021) Structure-guided multivalent nanobodies block SARS-CoV-2 infection and suppress mutational escape. Science 371(6530):6230. https://doi.org/10.1126/science.abe6230
57. Tian F, Tong B, Sun L, Shi S, Zheng B, Wang Z, Dong X, Zheng P (2021) Mutation N501Y in RBD of spike protein strengthens the interaction between COVID-19 and its receptor ACE2. BioRxiv
58. Kumar S, Karuppanan K, Subramaniam G (2022) Omicron (BA. 1) and sub-variants (BA. 1, BA. 2 and BA. 3) of SARS-CoV-2 spike infectivity and pathogenicity: a comparative sequence and structural-based computational assessment. bioRxiv. https://doi.org/10.1002/jmv.27927
59. Han P, Li L, Liu S, Wang Q, Zhang D, Xu Z, Han P, Li X, Peng Q, Su C, Huang B (2022) Receptor binding and complex structures of human ACE2 to spike RBD from omicron and delta SARS-CoV-2. Cell 185(4):630–640. https://doi.org/10.1016/j.cell.2022.01.001
60. Maestro S (2020) Maestro. Schrödinger LLC, New York
61. Gai J, Ma L, Li G, Zhu M, Qiao P, Li X, Zhang H, Zhang Y, Chen Y, Ji W, Zhang H (2021) A potent neutralizing nanobody against SARS-CoV-2 with inhaled delivery potential. MedComm 2(1):101–113. https://doi.org/10.1002/mco2.60
62. Naik B, Gupta N, Ojha R, Singh S, Prajapati VK, Prusty D (2020) High throughput virtual screening reveals SARS-CoV-2 multi-target binding natural compounds to lead instant therapy for COVID-19 treatment. Int J Biol Macromol 160:1–17. https://doi.org/10.1016/j.ijbiomac.2020.05.184
63. Naik B, Mattaparthi VSK, Gupta N, Ojha R, Das P, Singh S, Prajapati VK, Prusty D (2021) Chemical system biology approach to identify multi-targeting FDA inhibitors for treating COVID-19 and associated health complications. J Biomol Struct Dyn. https://doi.org/10.1080/07391102.2021.1931451
64. Ferdinands JM, Rao S, Dixon BE, Mitchell PK, DeSilva MB, Irving SA, Lewis N, Natarajan K, Stenehjem E, Grannis SJ, Han J (2022) Waning 2-dose and 3-dose effectiveness of mRNA vaccines against COVID-19–associated emergency department and urgent care encounters and hospitalizations among adults during periods of Delta and Omicron variant predominance—VISION Network, 10 states, August 2021–January 2022. Morb Mortal Wkly Rep 71(7):255. https://doi.org/10.15585/mmwr.mm7107e2
65. Ojha R, Gupta N, Naik B, Singh S, Verma VK, Prusty D, Prajapati VK (2020) High throughput and comprehensive approach to develop multiepitope vaccine against minacious COVID-19. Eur J Pharm Sci 151:105375. https://doi.org/10.1016/j.ejps.2020.105375
66. Sharma V, Singh S, Ratnakar TS, Prajapati VK (2022) Chapter Immunoinformatics and reverse vaccinology methods to design peptide-based vaccines. In: Tripathi T, Dubey VK (eds) Advances in protein molecular and structural biology methods. Academic Press, Cambridge p, pp 477–487
67. Robson B (2020) COVID-19 Coronavirus spike protein analysis for synthetic vaccines, a peptidomimetic antagonist, and therapeutic drugs, and analysis of a proposed achilles' heel conserved region to minimize probability of escape mutations and drug resistance. Comput Biol Med 121:103749. https://doi.org/10.1016/j.compbiomed.2020.103749
68. Biswas M, Yamazaki T, Chiba J, Akashi-Takamura S (2020) Broadly neutralizing antibodies for influenza: passive immunotherapy and intranasal vaccination. Vaccines 8(3):424. https://doi.org/10.3390/vaccines8030424
69. Panda M, Kalita E, Singh S, Kumar K, Rao A, Prajapati VK (2022) MiRNA-SARS-CoV-2 dialogue and prospective anti-COVID-19 therapies. Life Sci. https://doi.org/10.1016/j.lfs.2022.120761
70. Chouhan P, Singh S, Sharma V, Prajapati VK (2022) Anti-IL-10 antibody humanization by SDR grafting with enhanced affinity to neutralize the adverse response of interleukin-10. Int J Pept Res Ther 28(5):148. https://doi.org/10.1007/s10989-022-10456-4
71. McCombs JR, Owen SC (2015) Antibody drug conjugates: design and selection of linker, payload and conjugation chemistry. AAPS J 17(2):339–351. https://doi.org/10.1208/s12248-014-9710-8

72. Li B, Tesar D, Boswell CA, Cahaya HS, Wong A, Zhang J, Meng YG, Eigenbrot C, Pantua H, Diao J, Kapadia SB (2014) Framework selection can influence pharmacokinetics of a humanized therapeutic antibody through differences in molecule charge. MAbs. https://doi.org/10.4161/mabs.29809
73. McConnell AD, Zhang X, Macomber JL, Chau B, Sheffer JC, Rahmanian S, Hare E, Spasojevic V, Horlick RA, King DJ, Bowers PM (2014) A general approach to antibody thermostabilization. MAbs. https://doi.org/10.4161/mabs.29680
74. Landry JP, Fei Y, Zhu X (2012) Simultaneous measurement of 10,000 protein-ligand affinity constants using microarray-based kinetic constant assays. Assay Drug Dev Technol 10(3):250–259. https://doi.org/10.1089/adt.2011.0406
75. Hacisuleyman A, Erman B (2019) ModiBodies: a computational method for modifying nanobodies to improve their antigen binding affinity and specificity. bioRxiv. https://doi.org/10.1007/s10867-020-09548-3
76. Jeong BS, Cha JS, Hwang I, Kim U, Adolf-Bryfogle J, Coventry B, Cho HS, Kim KD, Oh BH (2022) Computational design of a neutralizing antibody with picomolar binding affinity for all concerning SARS-CoV-2 variants. MAbs 14(1):2021601. https://doi.org/10.1080/19420862.2021.2021601